

THE PRESENT WORK WAS SUBMITTED TO THE INSTITUTE OF COMPUTATIONAL GEOSCIENCE,  
GEOTHERMIE UND RESERVOIRGEOPHYSIK

UNDERSTANDING APPARENT OUTLIERS IN  
LOW-TEMPERATURE THERMOCHRONOLOGICAL DATA IN  
THE SWISS SUBALPINE MOLASSE USING STRUCTURAL  
UNCERTAINTY MODELING

THESIS FOR OBTAINING THE ACADEMIC DEGREE  
MASTER OF SCIENCE (M.Sc.)

PRESENTED BY:  
**ZIEGLER, JOSEFINE**  
427203

*1<sup>st</sup>* EXAMINER:  
UNIV.-PROF. PH.D. FLORIAN WELLMANN  
INSTITUTE OF COMPUTATIONAL GEOSCIENCE, GEOTHERMIE UND RESERVOIRGEOPHYSIK,  
RWTH AACHEN

*2<sup>nd</sup>* EXAMINER:  
UNIV.-PROF. PH.D. CHRISTOPH VON HAGKE  
INSTITUTE OF GEOLOGY AND PHYSICAL GEOGRAPHY, PLUS SALZBURG

AACHEN, JANUARY 2023



# Eidesstattliche Versicherung

## Statutory Declaration in Lieu of an Oath

---

Ziegler, Josefine

Name, Vorname/Last Name, First Name

---

427203

Matrikelnummer (freiwillige Angabe)

Matriculation No. (optional)

Ich versichere hiermit an Eides Statt, dass ich die vorliegende ~~Arbeit/Bachelorarbeit/~~  
Masterarbeit\* mit dem Titel

I hereby declare in lieu of an oath that I have completed the ~~present paper/Bachelor thesis/Master thesis\*~~ entitled

Understanding apparent outliers in low-temperature thermochronological data in the

Swiss Subalpine Molasse using structural uncertainty modeling

---

selbstständig und ohne unzulässige fremde Hilfe (insbes. akademisches Ghostwriting) erbracht habe. Ich habe keine anderen als die angegebenen Quellen und Hilfsmittel benutzt. Für den Fall, dass die Arbeit zusätzlich auf einem Datenträger eingereicht wird, erkläre ich, dass die schriftliche und die elektronische Form vollständig übereinstimmen. Die Arbeit hat in gleicher oder ähnlicher Form noch keiner Prüfungsbehörde vorgelegen.

independently and without illegitimate assistance from third parties (such as academic ghostwriters). I have used no other than the specified sources and aids. In case that the thesis is additionally submitted in an electronic format, I declare that the written and electronic versions are fully identical. The thesis has not been submitted to any examination body in this, or similar, form.

---

León, 27.02.2023

Ort, Datum/City, Date

---



Unterschrift/Signature

\*Nichtzutreffendes bitte streichen

\*Please delete as appropriate

**Belehrung:**

Official Notification:

**§ 156 StGB: Falsche Versicherung an Eides Statt**

Wer vor einer zur Abnahme einer Versicherung an Eides Statt zuständigen Behörde eine solche Versicherung falsch abgibt oder unter Berufung auf eine solche Versicherung falsch aussagt, wird mit Freiheitsstrafe bis zu drei Jahren oder mit Geldstrafe bestraft.

**Para. 156 StGB (German Criminal Code): False Statutory Declarations**

Whoever before a public authority competent to administer statutory declarations falsely makes such a declaration or falsely testifies while referring to such a declaration shall be liable to imprisonment not exceeding three years or a fine.

**§ 161 StGB: Fahrlässiger Falscheid; fahrlässige falsche Versicherung an Eides Statt**

(1) Wenn eine der in den §§ 154 bis 156 bezeichneten Handlungen aus Fahrlässigkeit begangen worden ist, so tritt Freiheitsstrafe bis zu einem Jahr oder Geldstrafe ein.

(2) Straflosigkeit tritt ein, wenn der Täter die falsche Angabe rechtzeitig berichtigt. Die Vorschriften des § 158 Abs. 2 und 3 gelten entsprechend.

**Para. 161 StGB (German Criminal Code): False Statutory Declarations Due to Negligence**

(1) If a person commits one of the offences listed in sections 154 through 156 negligently the penalty shall be imprisonment not exceeding one year or a fine.

(2) The offender shall be exempt from liability if he or she corrects their false testimony in time. The provisions of section 158 (2) and (3) shall apply accordingly.

Die vorstehende Belehrung habe ich zur Kenntnis genommen:

I have read and understood the above official notification:

---

León, 27.02.2023

Ort, Datum/City, Date

---

  
Unterschrift/Signature



## **Acknowledgement**

Throughout my work on this thesis I received great support. I want thank my supervisor Prof. Florian Wellmann for giving me a lot of freedom with regards to the aim of this thesis, while always providing constructive criticism and a broader view on the topic.

I thank my supervisor Prof. Christoph von Hagke for the opportunity of writing about this topic and the guidance throughout the thesis.

In addition, I also want to thank Sofia Brisson for bringing me into her PhD project and mentoring me throughout my master thesis and lastly Maxwell Angel, for taking care of printing and handing in the final work.

## **Abstract**

Thermochronological data and kinematic models are often combined to retrace exhumation, cooling, or fault activity. However, structural uncertainty is often neglected in thermokinematic models, which can lead to bias when interpreting data. Here we aim to test the influence of structural uncertainty on the interpretation of low-temperature thermochronological data in Mount Rigi in the Swiss Subalpine Molasse, a key region in the Swiss foreland fold-thrust belt of the European Alps. The region has been incorporated into the Alpine orogenic wedge in the Miocene, which led to the development of a triangle zone at the leading edge of deformation. An extensive low-temperature thermochronological data set exists, including apatite fission track as well as apatite (U-Th)/He data, which contains outliers not easily explained by existing kinematic models.

To diminish bias in the thermokinematic model we first estimated the geological uncertainty by computing and comparing 1000 stochastically generated 3D implicit geometric models, varied within an assigned uncertainty range assigned to geological input parameters. Model generation is performed with the stochastic geological modeling engine implemented in the Python package GemPy. In a second step a kinematic model was created which was designed to have minimal exhumation rates. With this setup, minimum values of cooling associated with shortening within the fold-thrust belt can be determined. Several samples have a cooling signal which must have had other influences than shortening. Here other processes responsible for cooling were discussed, such as erosion caused by drainage reorganization, or uplift and erosion due to deep-seated processes. Additionally, hydrothermal fluids are taken into account for explaining individual data points. With this research, I am giving new insights into the temporal evolution of heat flow in foreland basins and show how including geological uncertainty can lead to better-constrained time-temperature histories.

# Contents

<b>1. Introduction</b>	<b>1</b>
<b>2. Methods and Material</b>	<b>3</b>
2.1. Geological setting . . . . .	3
2.1.1. Geology of the North Alpine Foreland Basin . . . . .	3
2.1.2. Stratigraphy of the North Alpine Foreland Basin . . . . .	5
2.1.3. Geological interpretations of the study area . . . . .	5
2.2. Geometric and probabilistic modeling . . . . .	6
2.2.1. Step 1: Geometric model . . . . .	6
2.2.2. Step 2: Uncertainty estimation . . . . .	9
2.2.3. Step 3 + 4: Simulation and computation of probabilistic model . . . . .	9
2.2.4. Step 5: Visualization . . . . .	9
2.3. Kinematic modeling . . . . .	10
2.4. Thermochronology . . . . .	12
<b>3. Results</b>	<b>14</b>
3.1. Geometric and probabilistic modeling . . . . .	14
3.2. Kinematic modeling . . . . .	16
3.3. Exhumation and cooling rates . . . . .	18
<b>4. Discussion</b>	<b>20</b>
4.1. Limitations in the modelling processes . . . . .	20
4.1.1. Geometric and probabilistic model . . . . .	20
4.1.2. Kinematic model . . . . .	21
4.2. Exhumation rates . . . . .	22
4.3. Processes influencing cooling rates . . . . .	23
4.4. Hydrothermal flow in triangle zones and foreland basins . . . . .	25
4.5. Alteration of thermochronometers through hydrothermal fluids . . . . .	26
<b>5. Conclusion and outlook</b>	<b>26</b>
<b>A. Raw GemPy model</b>	<b>33</b>
<b>B. Thermochonological Data</b>	<b>34</b>

## List of Figures

1.	Spectrum of different modeling approaches: a) interpolation, b) kinematic modeling, c) process simulations (From Wellmann et al. (2016) after Jessell and Valenta (1996)) . . . . .	2
2.	Geological map of Swiss Subalpine Molasse, the modeled area is marked in red, for geological profiles of section (A-B) and (C-D) see fig. 4 a) and b). L: Luzern. Map after von Hagke et al. (2012) . . . . .	4
3.	Chronostratigraphic diagram of the North Alpine Foreland Basin in Central Switzerland (Schlunegger, 1999). OSM: Upper Freshwater Molasse, OMM: Upper Marine Molasse, USM: Lower Freshwater Molasse, UMM: Lower Marine Molasse . . . . .	6
4.	Three different geological profiles in the study area. a) Profile section "Entlebuch" (Section C-D fig. 2) (von Hagke et al., 2012), b) profile section "Rigi" (Section A-B in fig. 2) (Kaiser, 2018), c) balanced profile section of Mount Rigi in similar location as b) (Burkhard, 1990) . . . . .	7
5.	Simple implicit model of a fault processed with Gempy. a) 3D visualization, b) Profile section of the model, c) input data, the arrows show the orientation and the points resemble base of formation, d) scalar field. . . . .	8
6.	Simple model of a fault modeled with Noddy. In b) a horizontal layer was inserted to trace exhumation from this depth. . . . .	12
7.	Low-temperature thermochronological data in the studied area. Map C: mean (U-Th-Sm)/He ages, map D: central fission track ages. Ages in Ma; LA-ICP-MS: laser ablation–inductively coupled plasma–mass spectrometry; EDM: external detector method; FT: fission track (From von Hagke et al., 2012). . . . .	13
8.	Thermal modeling results from HeFTy for the samples discussed. The dark grey path represents better fits ( $GOF > 0.5$ ), the light grey path less likely fits ( $GOF > 0.05$ ). The boxes mark the time of deposition and post- or prepositional temperature constraints. The thick line at 10 Ma marks a cooling event which occurred in nearly all samples. (From von Hagke et al. (2012)) . . . . .	15
9.	Geometric model of the subsurface of the study area computed with GemPy and processed with Blender. . . . .	16
10.	Visualization of the information entropy of the geometric model a) 3D lithology blocks of the whole extent b) 3D fault blocks model of the whole extent, c) profile section along the red line in a) showing the entropy of the lithology blocks, d) profile section along the red line in b) showing the entropy of the fault blocks. . . . .	17
11.	Two kinematic realizations made using Noddy with similar but different fault geometry and resulting exhumation. For the difference in exhumation see tab. 3. . . . .	18
12.	One kinematic realization with faults producing the least amount of exhumation, while staying true to the surface geology. Each figure uses a different depth of the horizontal layer to show the exhumation of the samples. For depth, elevation, and exhumation see Tab. 3.3 . . . . .	19

13.	AFT and (U-Th-Sm)/He data plotted along the profile section. The numbers 1–4 refer to the tectonic slice. Data from Cederbom et al. (2004); von Hagke et al. (2012); Lindow (2009) . . . . .	24
14.	AFT and (U-Th-Sm)/He data plotted against elevation. Data from Cederbom et al. (2004); von Hagke et al. (2012); Lindow (2009) . . . . .	25
15.	GemPy model before being processed with Blender . . . . .	33

## List of Tables

1.	Summary of uncertainties assigned to all surfaces. ( $\sigma(z) = 0.11914 \cdot z + 218.32648$ m, $z$ refers to the depth) . . . . .	10
2.	Maximum, mean and minimum entropy (H) of the probabilistic model. . . . .	15
3.	Exhumation at the base of each fault of kinematic models a) and b), see fig. 11 for realizations. . . . .	16
5.	Thermochronological data used in this study . . . . .	34

## 1. Introduction

Structural geological models are the product of geological observations, such as, geological maps, well logs or geophysical measurements. These models resemble an interpretation of this data and there is great effort done to make these interpretations as realistic as possible. Especially in fold and thrust belts, like the Swiss Subalpine Molasse, with low relief, vegetation, settlements, and agriculture the geological interpretations rely on underground data. When geological models mainly rely on underground data there are usually several different interpretations, especially in areas of high structural complexity, which again is the case for the studied area (von Hagke and Malz, 2018). Geometric uncertainties are linked to kinematic interpretations, potentially leading to propagation of errors of greater magnitude.

Thermokinematic models use thermochronological data to constrain the order, rate, and date of geological events in kinematic models (Okaya et al., 1996). Thermochronology uses radioactive decay to date when a particle was cooled below the closure temperature of its thermochronometer (Reiners and Ehlers, 2018). With thermochronology the temperature a particle experienced can be put into a chronological frame. Thermokinematic models are common practice to learn more about the temporal evolution of a geological structure (see Okaya et al., 1996; Simoes et al., 2007; Berger and Bousquet, 2008; McQuarrie et al., 2008; Gehrels et al., 2011; Erdős et al., 2014). Structural uncertainties in these models are often excluded and not considered. However, taking manifold geological models into account is crucial to the interpretation of any data, because it can help to reduce our bias and introduce new theories (Wellmann and Regenauer-Lieb, 2012; Bárdossy and Fodor, 2001). Without incorporating structural uncertainty there is also no way to estimate the scope of error in the contribution of an individual exhumation driving mechanism.

Changing the input of events in kinematic models (e.g. dip, shape or depth of faults or the stratigraphy) produces different realizations of the geological evolution. Which in turn will have different exhumation and accordingly also different cooling rates, providing new and omitting old interpretations to thermochronological data.

Using the 3-D implicit geometric modeling approach GemPy is an advantage in this case, because implicit models consist of one scalar field for several geological surfaces. Whereas, in contrast explicit methods produce individual volumes which can lead to meshing complications when changing single data points a alter stage (de la Varga et al., 2019; Jessell et al., 2014; Wellmann and Caumon, 2018). With implicit modeling techniques this problem can be bypassed. Furthermore, GemPy takes basic geological principles into account, such as superposition and cross-cutting relationships, bringing more geological realism into these models. GemPys open source code makes the results more transparent compared to commercial softwares such as Leapfrog or Geomodeller (Newell, 2018).

Errors accumulate in geological models due to sparse data, imprecise measurements, missing knowledge, or bias (Bond, 2015). The sum of these errors is in the end considered geological uncertainty. Estimating these errors has therefore become a central part of geomodeling, as it helps to minimize and locate areas of high uncertainties (Wellmann et al., 2010; Wellmann and Caumon, 2018). For these purposes the advantages of implicit modeling are even more relevant. It enables to stochastically change individual data points without having to manually adjust for meshing errors or unrealistic geological realizations. By automizing these processes many geological models can be computed in

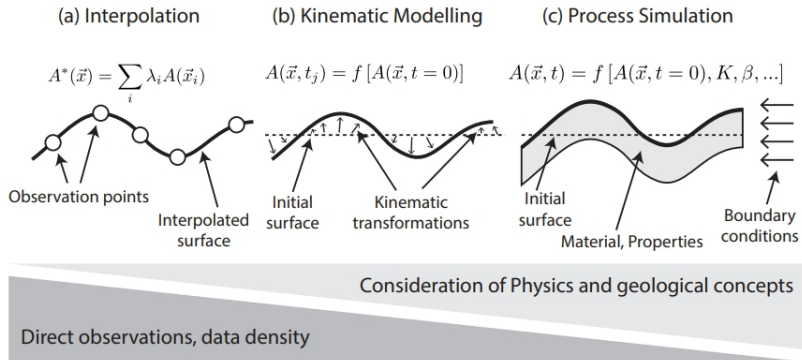


Figure 1: Spectrum of different modeling approaches: a) interpolation, b) kinematic modeling, c) process simulations (From Wellmann et al. (2016) after Jessell and Valenta (1996)).

little time and with less bias than interpreting, for example, a seismic section or several core logs by hand. Comparing these stochastically computed models generates new geological information and give deeper insight into the level of precision of our predictions throughout the subsurface.

The concept of geometric modeling focuses on giving the most accurate representation of geological observations (Fig. 1 a)) (see Jessell and Valenta, 1996; Wellmann et al., 2016). The tool used to make a geological model out of the data points is the interpolation method applied. Dynamic modeling approaches, in contrast, are simulations of physical processes with no input of geological observations (Fig. 1 c)). Here physical parameters of the materials and boundary conditions control the outcome. On a spectrum these two approaches are endmembers. Kinematic models are located in between, taking geological observations and physical parameters into account (Fig. 1 c)). Kinematic approaches are used to model tectonic events of a geological history by applying kinematic transformations to a surface (Jessell and Valenta, 1996; Brandes and Tanner, 2014; Wellmann et al., 2016). They determine the evolution of a model obtained through interpolation by applying the impact of material properties and boundary conditions. The kinematic transformations are vectors containing, for instance, the information on stratigraphy, stress, and strain (Brandes and Tanner, 2014). Due to the complex nature of geological observations simplifications have to be made in any geological model, depending on the models desired application. The 3D kinematic modeling program Noddy allows to build complex geological model as the product of a sequence of simple structural, igneous or sedimentary events (Jessel, 1981).

This idea is applied to a case study. The low-temperature thermochronological data presented by von Hagke et al. (2012) and Cederbom et al. (2004) describes the recent cooling history of the Swiss Subalpine Molasse at Mount Rigi. The data consists of a horizontal and vertical profile with (U-Th)/He and Apatite fission track (AFT) measurements. The data presented contains some outliers which do not fit in the expected pattern along a horizontal and vertical section (von Hagke et al., 2012, 2015). The horizontal section requires great displacement and erosion rates to explain the measured cooling ages, which do not seem feasible. There are also samples in a vertical section which do not seem to be the result of tectonic shortening. Comparing data from Mount Rigi to other areas within the Swiss Subalpine Molasse basin, another anomaly becomes apparent: The depth of the Partial annealing zone is located around 1500 m higher than compared to the wells Hünenberg or Boswil (Cederbom et al., 2004). Although often used to estimate exhumation and shortening rates,

thermochronology only records cooling rates. Cooling rates represent a geothermal gradient, which on the other side can be influenced by climate, tectonic shortening, igneous intrusions or hydrothermal flow. It remains unclear to which extent exhumation linked to tectonics is the driving mechanism of cooling in this area (Cederbom et al., 2004, 2011; Schlunegger and Mosar, 2011; von Hagke et al., 2012, 2015).

By considering structural uncertainty in a thermokinematic model, I want to give new insights into the recent thermal history of Mount Rigi in the Swiss Subalpine Molasse.

## 2. Methods and Material

### 2.1. Geological setting

#### 2.1.1. Geology of the North Alpine Foreland Basin

The area studied concentrates on Mount Rigi in Central Switzerland. It is part of the North Alpine Foreland Basin (NAFB). The tectonic history and stratigraphy of the study area are mainly influenced by the break up of Pangea and the collision of the African and Eurasian Plate that followed, resulting in the Alpine orogeny (Trümpy, 1960; Frisch, 1979; Tricart, 1984). The break up of Pangea produced a range of different sedimentary environments such as deep seas, shallow seas, and continental shelves, which are now often found in a seemingly chaotic arrangement in the Alps (Pfiffner, 2015). The Alps are divided into the Helvetic, Penninic, Austro Alpine, and southern nappes. North of the Alps the NAFB is stretching from eastern France to Vienna. The NAFB is a peripheral foreland basin, which formed due to the alpine orogeny and the resulting tectonic load and flexural bending of the Eurasian Plate (Allen and Homewood, 2009; Homewood et al., 1986; Sinclair et al., 1991).

Two regressive megacycles during the Paleogene and Neogene subsequently filled the basin, resulting in four formations: Upper Freshwater Molasse (OSM), Upper Marine Molasse (OMM), Lower Freshwater Molasse (USM), and Lower Marine Molasse (UMM) (Fig. 2.1.2) (Sinclair et al., 1991; Scholz, 2016).

The NAFB consists of two tectonic units: the (par)autochthonous Plateau Molasse and the allochthonous Subalpine Molasse (Trümpy et al., 1980). The border is marked by complimentary dipping faults and strata, both striking NE-SW. These outcropping faults share the same basal detachment and belong to the complex fault system of the underlying triangle zone (McClay, 1992). The exact geometry and amount of faults is uncertain (Burkhard, 1990; Kaiser, 2018; Allenbach, 2017). Matter of discussion is also the time when thrusting started. While thermochronological the faults being active 10–5 Ma ago, other suggestions are that thrusting started already in the Aquitanian and lasted until Langhian (Schlunegger et al., 1997; Schlunegger, 1999; von Hagke et al., 2012). The continuous tectonic stress initiated overthrusting of the Rigi thrust sheet, the imbrication of the Jura mountains, and propagation of faults into the Helvetic nappe (Schlunegger et al., 1997; Schlunegger, 1999; Rosenbaum et al., 2002; Pfiffner, 2015). The Helvetic nappe, found in the south of the study area, was (over)thrusted along the Axen thrust on top of the Subalpine Molasse (Pfiffner, 2015).

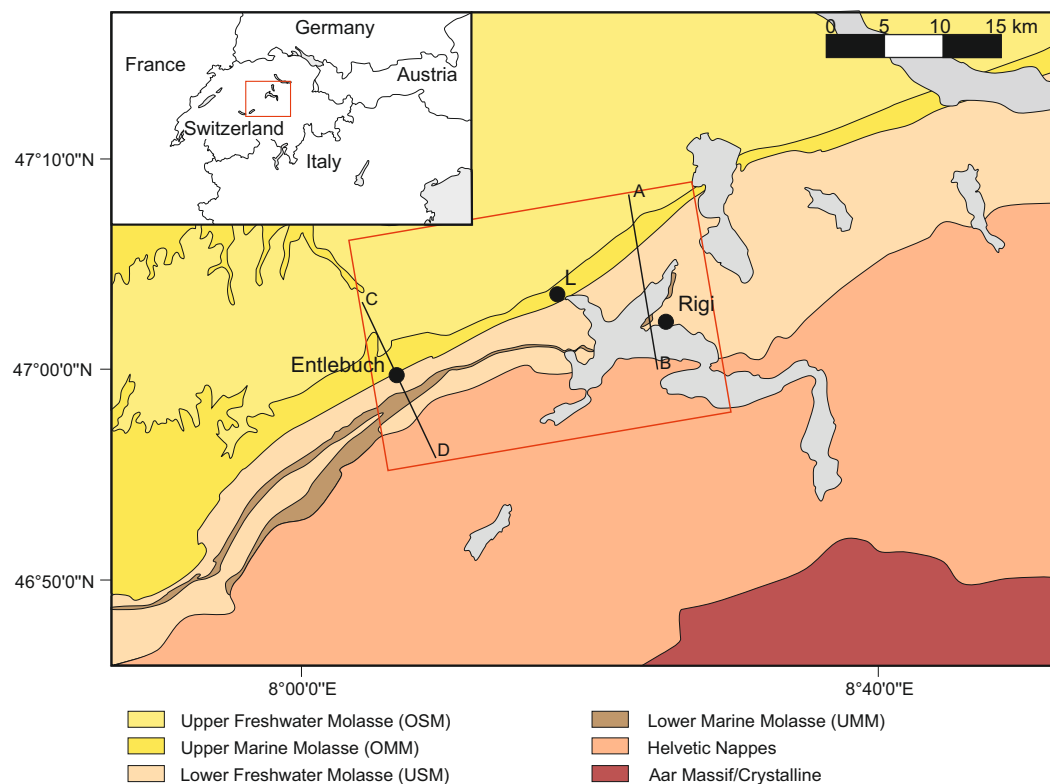


Figure 2: Geological map of Swiss Subalpine Molasse, the modeled area is marked in red, for geological profiles of section (A-B) and (C-D) see fig. 4 a) and b). L: Luzern. Map after von Hagke et al. (2012)

### **2.1.2. Stratigraphy of the North Alpine Foreland Basin**

The stratigraphy of foreland basins is controlled by the interplay of tectonic processes and the erosion of the growing orogen. Erosion of the orogen alters the basin geometry by redistributing and balancing the load on the subducted plate, controlled by deflection of the plate and slope of the wedge (Sinclair et al., 1991). The NAFB is characterized by two regressive shallowing and coarsening upwards megacycles from marine to freshwater environments (Sinclair et al., 1991; Scholz, 2016). The Swiss UMM (36 - 27 Ma) consists of turbidites in the middle and limestones and glauconitic sandstones at the top. It is only outcropping in the Subalpine Molasse (Sinclair et al., 1991; Sinclair, 1997; Homewood et al., 1986). The very bottom, is made up of shaly sandstone with conglomeratic intercalations. The middle unit is called Grisigen Marl and composed of layered clayey marl and siltstones. These marls acted as detachment horizon of faults propagating into the triangle zones. The sandstones on top are interpreted as the transition to a more terrestrial environment of the basin, having a gradual contact with the USM (Holliger, 1955).

The USM (29 - 22 Ma) is dominated by fluvial-terrestrial sediments, the result of a worldwide sea-level fall. The thickness thins to the North from 4 km thick deposits in the South, to 300 m or less close to the Jura province (Homewood et al., 1986). Trümpy et al. (1980) documented seven alluvial fans in the USM along the northern margin of the Alps. They are made up of conglomerates, which are interfingered with silty marls at their limits. The clasts of the Rigi and Speer fans were derived from Cretaceous Penninic and Ultra-Penninic flysch (Sinclair et al., 1991; Homewood et al., 1986). With time these talus cones progradated northwards towards the basin axis and coarse material was deposited above finer grained (Pfiffner, 2015). Periods with drier climate are marked by playa sediments and scattered saline lakes (Homewood et al., 1986).

With the onset of the Burdigalian the NAFB was flooded from East and West and marine conditions were re-established between the Rhone Basin and Vienna Basin, marking the base of the OMM (16 - 11 Ma) (Trümpy et al., 1980; Sinclair et al., 1991; Scholz, 2016). At the southern border of the sedimentary environment two large deltaic fans dominate the OMM in Switzerland (Napf fan and Hörnli fan), where sediments from the approaching Alps were deposited (Allen et al., 1985).

By the upper Burdigalian the sea retreated to the west. This marks the beginning of deposition of the OSM (16 - 11 Ma). Coarse terrestrial sediments dominate the gravel fans, with sandy and silty grain-sizes deposits in between. Some formations also show local coal seams and freshwater carbonates (Trümpy et al., 1980; Sinclair et al., 1991). In the more recent geological history the landscape was shaped by the Quaternary ice ages (Scholz, 2016). They left behind steep valleys which were filled with sediments and moraines. Due to the proximity of the Alps only sediments from the last ice age, the Würm period, are found today.

### **2.1.3. Geological interpretations of the study area**

The surface geology of the study area has been mapped in great detail by the Swiss authorities and several geological interpretations of the subsurface have been done (swisstopo; Burkhard, 1990; Kaiser, 2018) (Fig. 4). Comparing fig. 4b) and c) shows how structurally different they can be, although both were made using seismic sections. For a more detailed discussion of the differences see section 4.1.1.

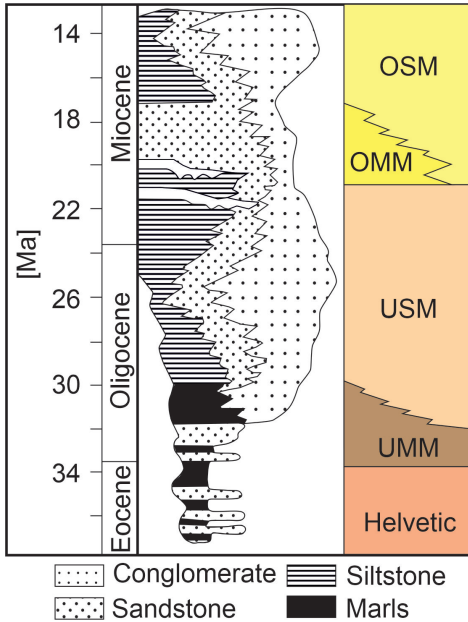


Figure 3: Chronostratigraphic diagram of the North Alpine Foreland Basin in Central Switzerland (Schlunegger, 1999). OSM: Upper Freshwater Molasse, OMM: Upper Marine Molasse, USM: Lower Freshwater Molasse, UMM: Lower Marine Molasse

In these profiles the structural complexity of the underlying triangle zone is visible. Fig. 4 a) and b) were chosen as the basis of the geological models. Fig. 4 b) was chosen due to its smaller structural complexity and the already existing estimation of structural uncertainty in Kaiser (2018)

## 2.2. Geometric and probabilistic modeling

The model was built following the 5 steps from Wellmann et al. (2010). Step 1 is constructing the initial model. This realization is considered as the best possible model, when taking all data available and knowledge into account. It also defines all relevant parameters such as extent, number of faults and stratigraphy (see section 2.2.1). In step 2 the quality of input data is evaluated and probability distributions are assigned to the location and orientation of data points. Step 3 consists of simulating new data sets with the uncertainties determined in step 2. In step 4 multiple models of the different realizations are being constructed which are then visualized, processed and analysed in step 5.

### 2.2.1. Step 1: Geometric model

The geometric and probabilistic model was processed with GemPy, an open-source 3D modeling tool for implicit geological models by de la Varga et al. (2019). The input data consists of points and orientations, which are assigned to one or more series of lithologies and faults. While the points resemble the base of a layer, the orientations are merely assigned to the layers and give information about the dip and azimuth (Fig. 5 c). GemPy considers geological surfaces as iso-surfaces in a scalar field  $S(x)$  (Fig. 5 d). These iso-surfaces connect the points of the single formations and are perpendicular to the orientations assigned. To interpolate between the points it uses universal cokriging, a method introduced by Lajaunie et al. (1997). Faults are accounted by generating drift functions which alter the

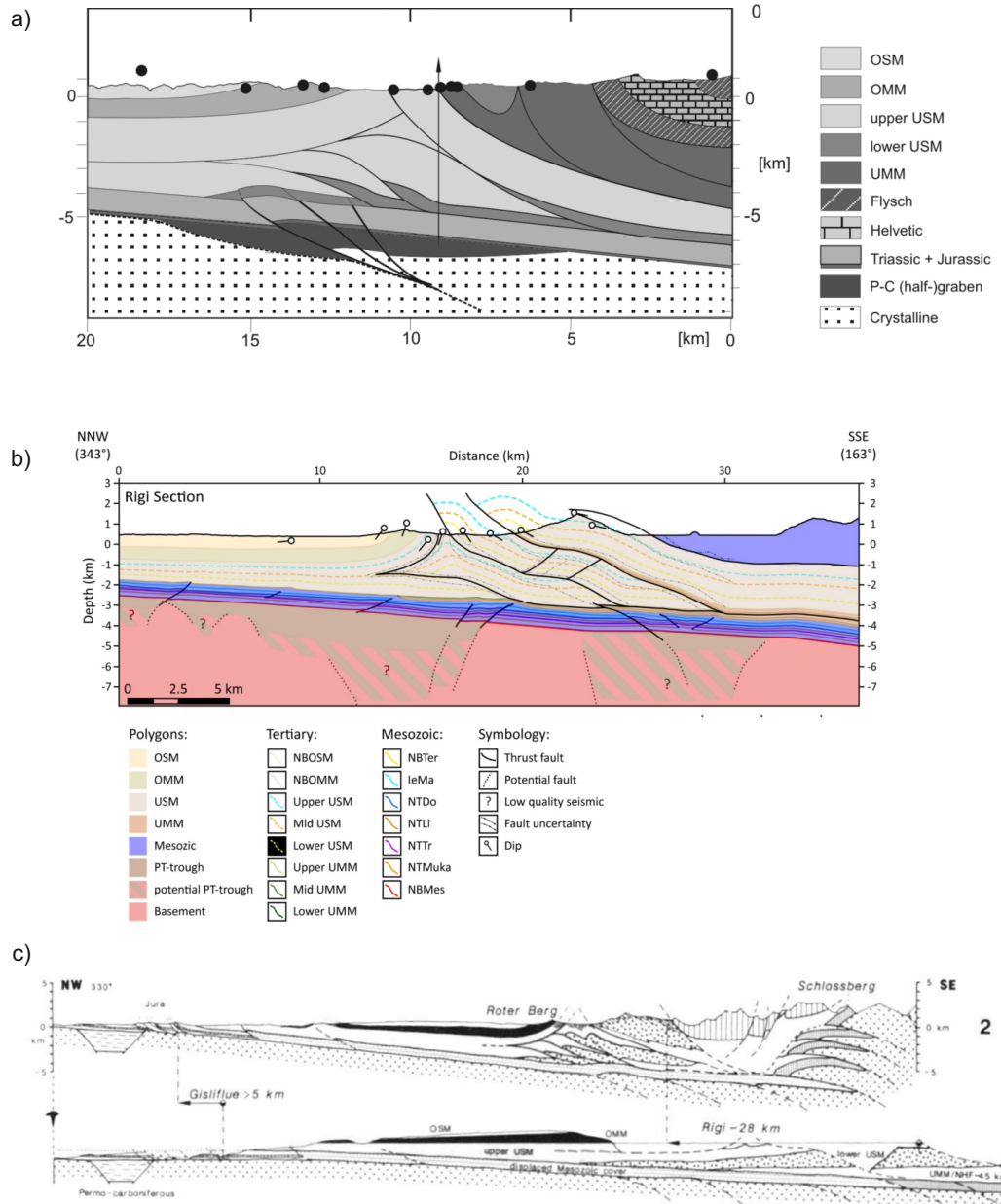


Figure 4: Three different geological profiles in the study area. a) Profile section "Entlebuch" (Section C-D fig. 2) (von Hagke et al., 2012), b) profile section "Rigi" (Section A-B in fig. 2) (Kaiser, 2018), c) balanced profile section of Mount Rigi in similar location as b) (Burkhard, 1990)

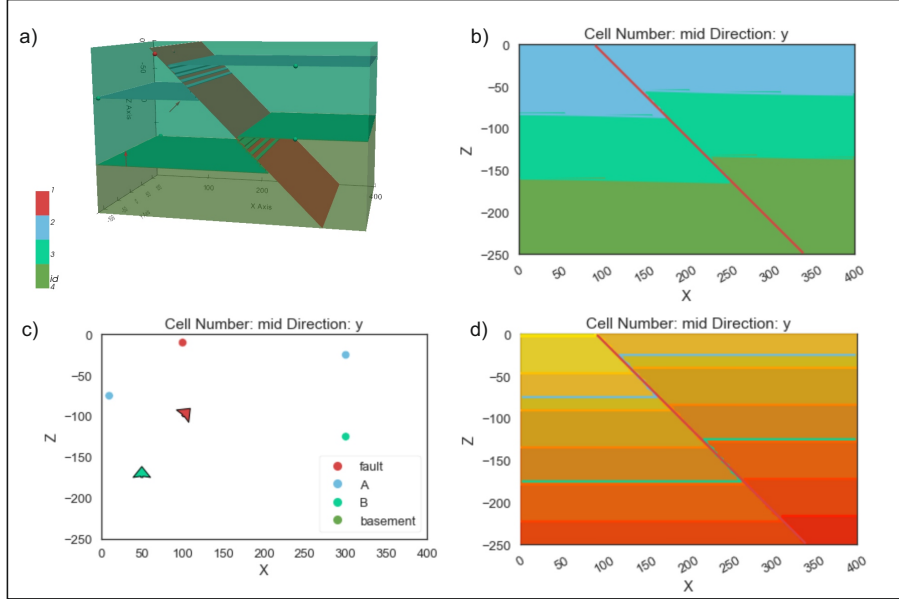


Figure 5: Simple implicit model of a fault processed with Gempy. a) 3D visualization, b) Profile section of the model, c) input data, the arrows show the orientation and the points resemble base of formation, d) scalar field.

scalar field in a restricted area while conserving its continuity. This enables the program to compute only one scalar field with consistent layers.

The stratigraphic pile contains the two regressive megacycles of the Molasse Basin, the Helvetic Nappe and further non-classified Mesozoic units (Fig. 3). The data was obtained from geological cross sections from von Hagke et al. (2012) and Kaiser (2018), the wells in Hünenberg and Entlebuch and geological maps (swisstopo; Greber et al., 1994), SEAG). The cross sections were digitized with Q-GIS and processed further using GemGIS to extract all data ready to be used as input for GemPy (Juestel et al., 2021). The model contains various simplifications: a) no unconformities were considered and all layers are part of the same potential field, b) several smaller faults from the profiles were not included due to limitations in the implicit modeling method and differences in the two profiles, c) the UMM was combined with the USM due to its small scale, d) every layer thickness was assumed to be more less homogeneous although the thickness varies especially in the Rigi fan, and e) the Rhenodanubian Flysch and Mesozoic sediments were not further differentiated. This leaves the model containing 5 faults and 5 lithologies (6 including the basement) in total. To correct for interpolation artefacts and missing data, points and orientations were added by hand. The extent of the model is  $x = 79 \text{ km}$ ,  $y = 53 \text{ km}$ ,  $z = 7550 \text{ m}$  with a resolution of  $100 \times 100 \times 50$ , or 500,000 voxels. The resolution in z was set to 50 to save on computing power. In a last step the model was compared to the 3D geological model of Switzerland by Allenbach (2017) to cross-check with data which was not being used for the model. For better visualization the model was processed using Blender, a free and open-source 3D graphic software.

## **2.2.2. Step 2: Uncertainty estimation**

Uncertainties in the raw data are being transferred to the model by errors in orientations and location of contacts or faults in the subsurface. Wellmann et al. (2010) defined three different types of uncertainties in geological models: a) uncertainty in the raw data used for modeling, b) stochastic errors resulting from inter- or extrapolation between/from known data points and c) imprecise or missing knowledge. The uncertainties are expressed through different forms of probability distribution with a standard deviation  $\sigma$ , depending on the type and depth of the geological structure. To characterize uncertainty of a gradual contact between two formations a normal distribution was chosen, for a missing direct contact (eg. vegetation, core loss, etc.) a continuous uniform distribution is used (Wellmann et al., 2010).

The standard deviations of the faults were determined after Kaiser (2018) (see Table 1). Kaiser (2018) quantified the uncertainty of the location and geometry of faults in the area of Mt. Rigi according to the intensity and continuity of seismic marker horizons from seismic profiles he interpreted. The Entlebuch profile did not contain any quantification of uncertainties, therefore the same uncertainties were assumed as in the Rigi profile.

The methods for assigning standard deviations, drawing random values and computing the new model were adapted from Brisson et al. (N.D.) with only minor changes. Points above 550 m MSL will be referred to as surface points, whereas points below will be referred to as subsurface. Surface points are considered to be more certain, since more data is available, which is usually also of better quality. With depth the quality of seismic profiles linearly decreases, which corresponds to higher uncertainty in the resulting structural interpretations (Schaaf and Bond, 2019). Therefore, the standard deviation must be greatest at the bottom of the model, in this case 6560 mbsl. Here the maximum standard deviation was assigned  $\sigma_{max} = 1000$ . Assuming  $\sigma_{min} = 100$  m for the topmost subsurface points (549 masl), the standard deviation is described by  $\sigma(z) = 0.11914 \cdot z + 218.32648$  m. The study area was intensely faulted after deposition, therefore the uncertainty also increases in X and Y direction with a set  $\sigma$ . Surfaces considered more uncertain are accounted for by multiplying  $\sigma(z)$  by 1.5 or 2. These surfaces are fault 3 and 4 (Kaiser, 2018). The random values estimated from  $\sigma(z)$  were drawn from a normal distribution.

The random values for surface points were drawn from a uniform distribution, because contacts can often not be precisely traced at the surface due to vegetation or buildings. Faults 3 and 4 were attributed a standard deviation of  $\sigma = 200$  and the others  $\sigma = 150$ .

## **2.2.3. Step 3 + 4: Simulation and computation of probabilistic model**

In step 3, 1000 new input data sets were created by drawing new data points, based on the assigned  $\sigma$  of each surface. In step 4 these models were then computed.

## **2.2.4. Step 5: Visualization**

In a final step, the results from step 4 were visualized using the method of Brisson et al. (N.D.) based on information entropy by Wellmann and Regenauer-Lieb (2012) and Shannon (2001). Information

Table 1: Summary of uncertainties assigned to all surfaces. ( $\sigma(z) = 0.11914 \cdot z + 218.32648$  m,  $z$  refers to the depth)

Surfaces	Depth	Position	Standard Deviation	Distribution Type
Fault 1, Fault 2, Fault 3	<550 m	X,Y	$\pm \sigma(z)$	normal
		Z	$\pm 2\sigma(z)$	normal
	>550 m	X,Y	$\pm 200$	uniform
		Z	$\pm 200$	uniform
Other surfaces	<550 m	X,Y	$\pm \sigma(z)$	normal
		Z	$\pm \sigma(z)$	normal
	>550 m	X,Y	$\pm 150$	uniform
		Z	$\pm 150$	normal

Entropy  $H$  is expressed as the sum of all  $N$  products of the probability of every possible outcome  $p_i$  and its logarithm:

$$H = - \sum_i^N p_i \log(p_i) \quad (1)$$

Every voxel in a model contains only one lithology but more than one fault is possible. Comparing the same voxel from all models from step 4 produces a stochastic distribution of the lithologies and faults, which is regarded as a measure of uncertainty. When there is only one possible outcome  $p_i = 1$ , then  $H_i = 0$ . For a voxel<sub>i</sub> with the same possibility of two or more formations,  $H$  will be maximal. This means for voxels with more than one outcome,  $H$  will be higher than for voxels with less possible lithologies or faults. Knowing the entropy of every voxel, an average entropy of the whole model can be computed. Due to the different types of surfaces regarding faults and formations, the visualization is carried out separately. They will be referred to as fault blocks and lithology blocks.

### 2.3. Kinematic modeling

The kinematic model was built using Noddy, a 3D geological and geophysical modeling software. Noddy lets the user create a complex model by stringing together simple events such as structural, sedimentary and igneous events (Jessel, 1981; Jessell and Valenta, 1996). First a layered stratigraphic pile is built which can then be altered by different events, for example: folding, faulting, unconformities, shear, igneous intrusions, strain, tilting, or foliation. These events can be individualized by several input parameters. In the end a cross section and map showing the lithology or signals of the assigned geophysical rock properties are calculated. The Python wrapper pynoddy enables to easily perform experiments on Noddy models (Wellmann et al., 2016).

The extent of this model is smaller (36.6 km x 5 km x 7 km) than that of the GemPy model and it is focused on the subsurface of Rigi (see section A-B in Fig. 2). While the extent and individual layers are true to scale, the orientation of the section is E-W and not NNW-SSE as in the map, therefore the strike of individual structures is not true to real geology. This was done to simplify the modeling process and allow for better visualization in the end. The sequence of events was determined after Kaiser (2018) and Schlunegger (1999):

1. Building the stratigraphic pile
  - a) Adding the Mesozoic layer at -2500 m

- b) Tilting the block by (090/0.1)
  - c) Applying an unconformity (000/00) at -1800 m, adding UMM to the stratigraphic pile
  - d) Applying an unconformity (270/0.5) at -1700 m, adding USM to the stratigraphic pile
  - e) Tilting the block (090/03)
  - f) Applying an unconformity (090/0.3) at -700 m, adding OMM and OSM at -10 m to the stratigraphic pile
2. Adding a horizontal layer (000/00) at an arbitrary depth using the dyke function, this will be changed later in pynoddy to trace the exhumation path of particles
  3. Adding fault 4 (Rigi Base thrust)
  4. Adding fault 3
  5. Adding fault 2 (Detachment) and fault 1 (Backthrust)
  6. Reactivating fault 3
  7. Reactivating fault 4

When defining an initial stratigraphic pile, Noddy only allows horizontal layers. However, the layers were not horizontal and homogeneous before deformation. By tilting and applying unconformities the filled NAFB with layers of differing thickness was represented. However, the strike and dip values in the profile section in Noddy do not represent the true values. All faults were implemented as a curved fault, which lets the user define the shape of the fault by drawing a profile. Since this profile could not be copied, the reactivated faults are merely an approximation of the initial fault. The other parameters were adjusted to achieve the desired outcome, for an accurate description of the implemented faults see t.

As well as in the GemPy model various simplifications were made: a) fault 1 and 2 were implemented as two events with a similar slip to resemble the tectonic wedge with little to no shortening and b) the Helvetic unit was not considered because this part of the area is not of interest and incorporating it in the stratigraphic pile would not have been possible.

The horizontal layer inserted was used to estimate the exhumation of a particle (Fig. 6). This simple model contains 3 layers of stratigraphy and one horizontal layer. In Fig. 6a) the depth from which particles were exhumed to the surface is not unambiguous. By inserting a horizontal layer at -2380 m depth (Fig. 6b)) the path of the exhumed particles and shape of the fault become clearer. In this model there is also a small artefact of the green formation, only visible in Fig. 6a) and in b) the deformation in the brown formation also becomes visible. The distance between horizontal layer and fault is different at the top of the profile to where the horizontal layer is cut off. This effect of thinning or stretching is also visible when comparing the distance from the horizontal layer to the top of the brown formation at the top of the profile and the undeformed layer.

With the framework outlined above, several realizations were made by altering the shape of the faults while taking into account the results of the probabilistic model. The constraint for accepting these models was their accuracy of representing the surface geology from Kaiser (2018) and maps swisstopo. The main structure of the model was kept the same, no more faults were added. The slip

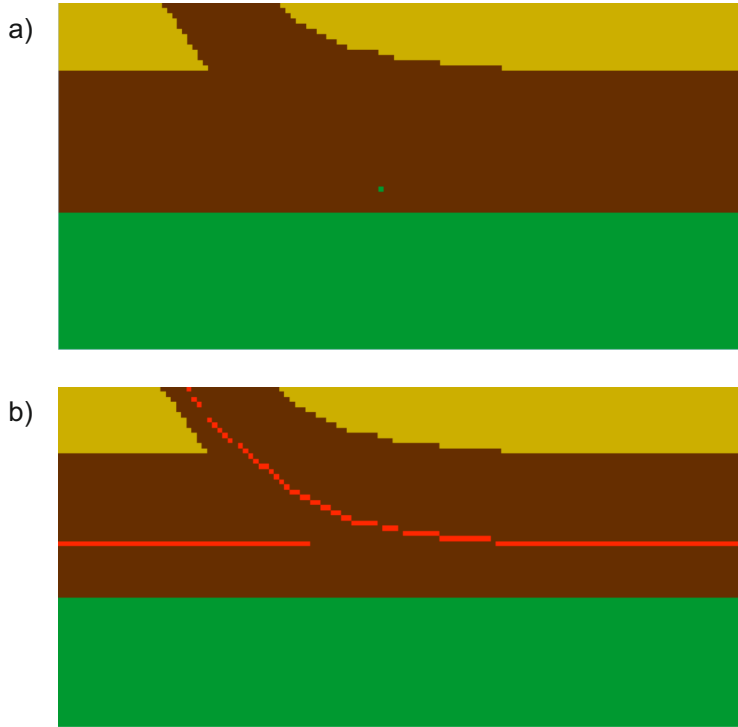


Figure 6: Simple model of a fault modeled with Noddy. In b) a horizontal layer was inserted to trace exhumation from this depth.

of the faults was always kept minimal. After finding the realization with the least exhumation on each fault the horizontal layer was moved upwards in increments starting at -3300 m using pynoddy (Wellmann et al., 2016). Then the locations of thermochronological data points from von Hage et al. (2012) were projected onto the profile. When the horizontal layer reached a data point, the exhumation was calculated by subtracting the depth of the horizontal layer from the elevation of the sample.

## 2.4. Thermochronology

Thermochronology is a common method to determine cooling paths of particles. There are several different thermochronometers, the ones most often used for low-temperature thermochronology are fission tracks and (U-Th-Sm)/He of apatite and zircons. Fission track (FT) uses narrow damage trails (fissures) in the crystal lattice caused by spontaneous radioactive decay of  $^{238}\text{U}$ . With elapsing time these fissures accumulate. However, when the crystal is heated above a specific closing temperature, the fissures begin to shorten (partial annealing) and at some point entirely heal (totally annealed). The depth where partial annealing is taking place is called the partial annealing zone (Reiners and Ehlers, 2018; Carlson et al., 1999).

The (U-Th-Sm)/He method measures the amount of  $^4\text{He}$  in a crystal, which is the decay product of  $^{238}\text{U}$ ,  $^{235}\text{U}$ ,  $^{232}\text{Th}$ , and  $^{147}\text{Sm}$ .  $^4\text{He}$  accumulates in the crystal over time, only if the crystal is heated above its closure temperature the  $^4\text{He}$  can diffuse out of the crystal and leave the system. The depth in

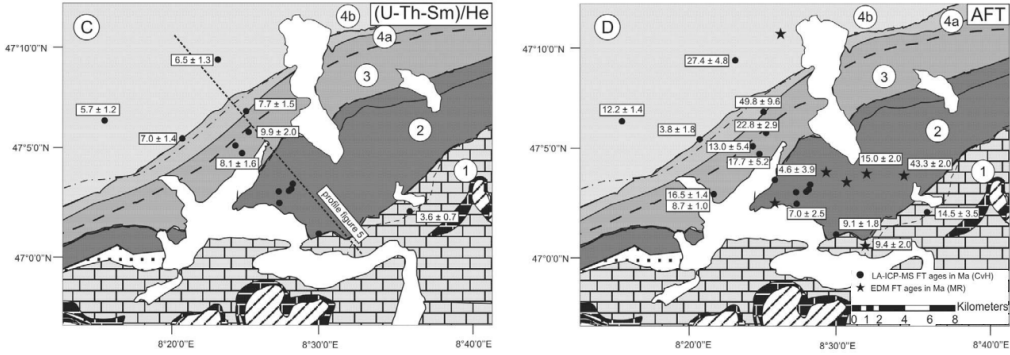


Figure 7: Low-temperature thermochronological data in the studied area. Map C: mean (U-Th-Sm)/He ages, map D: central fission track ages. Ages in Ma; LA-ICP-MS: laser ablation–inductively coupled plasma–mass spectrometry; EDM: external detector method; FT: fission track (From von Hagke et al., 2012).

which the (U-Th-Sm)/He system is sensitive is called the partial retention zone (Reiners and Ehlers, 2018; Fitzgerald et al., 2006; Chew and Spikings, 2015).

Exhumation refers to the vertical component of the upward movement of a particle. It goes hand in hand with cooling, since the temperature of the Earth rises the deeper it gets. Although cooling is often linked to exhumation, it is important to keep in mind that thermochronometers measure solely a cooling signal, which can also be related to other processes than exhumation (Reiners and Ehlers, 2018).

The thermochronological data used consists of apatite FT (AFT) and apatite (U-Th-Sm)/He data. AFT records temperatures between 60–120°C and (U-Th-Sm)/He records 40–80°C, the exact closing temperature however depends on the chemical composition of each grain. Together FT and (U-Th-Sm)/He form a powerful tool to understand the low-temperature history of a sample (Carlson et al., 1999; Fitzgerald et al., 2006). Dating several samples along a horizontal profile demonstrates the cooling rates of both thermochronometers depending on the distance to the fault, dip, and exhumation rate (von Hagke et al., 2012). Closer to the fault both ages will be identical, in case they were both fully reset and annealed. Farther away from the fault, first the AFT age will be getting older and then also the apatite (U-Th-Sm)/He age, until they both reach the age of the footwall (von Hagke et al., 2012). The thermochronological data (Fig. 7) used in this study was obtained and interpreted by von Hagke et al. (2012).

The geological map was divided into four different tectonic slices (TS), confined by faults. In TS 2, 3, and 4 all samples were completely reset/annealed or strongly reset/annealed (von Hagke et al., 2012). This is indicated by thermochronological ages younger than their stratigraphical age, implying heating after deposition. For a detailed discussion of each sample, the reader is referred to von Hagke et al. (2012).

To connect thermochronological ages to exhumation the geothermal gradient has to be known. For depths until 1000 m below sea level (mbsl) a geothermal gradient of 30°C was assumed and for greater depths 22°C (Cederbom et al., 2004; Rybach, 1992). The mean annual temperature in this region is 9°C, this was added to the obtained temperature at depth (MeteoSwiss). In a next step these calculated

temperatures were compared to t-T paths of each sample modeled with HeFTy (Fig. 8). HeFTy is an inverse and forward modeling program for low-Temperature thermochronology data (fission track, U-Th-He, vitrinite reflectance) (Ketcham, 2005; Vermeesch and Tian, 2014). It computes possible t-T paths which fit to the measurements of thermochronological analyses. Using these models time and temperatures of heating and cooling can be determined.

## 3. Results

### 3.1. Geometric and probabilistic modeling

Although simplified, the geological model still gives a good representation of the underlying geology, especially the placement of the faults aligns with the interpretation of the geology of the area (Fig. 15). Only their trend in the very east of the model should be directed more to the East instead of the North. The different layers of lithology does not represent the geology well, especially inside the triangle zone. In the profiles used to as input only USM is interpreted inside the triangle zone, while in the geometric model there are artefacts of the underlying Mesozoic unit, OSM, and OMM. Furthermore, the Helvetic unit was extrapolated to lie on top of the OSM in the North and the OSM and OMM were also extrapolated South of the triangle zone, although no points or orientations were given which indicate this. Also the stratigraphic pile is wrong and GemPy regarded the Helvetic unit as the youngest one.

The GemPy model was then processed with Blender for visualization purposes (Fig.9). This step is necessary to free the model of artifacts and provide a more accurate representation of the underlying geology. During this processing, the faults were barely altered, but the lithology was altered in the previously mentioned areas.

The visualization of the probabilistic model (Fig. 10) shows the areas of highest entropy of the lithology and the faults. The lithology block has a greater mean entropy, while the maximum is greater in the fault block (see table 2). The greatest entropy in the lithology block can be attributed to a) areas close to faults, b) along fault 4 in the Rigi view and faults 1 and 3 in the Entlebuch view, c) areas of higher structural complexity, and d) areas of computing artefacts. These artefacts are in the north and along the outcropping faults of the triangle zone, especially fault 3. The highest entropy in the fault block is found along faults 1 and 2 in the very north. In both profile sections a general trend of higher uncertainty towards greater depth can be observed.

The profile section shows high entropy where fault 1 and 2 intersect ( $Y = 5.190\text{e}6$  m) and where faults 2, 3 and 4 meet ( $Y = 5.215 - 5.225\text{e}6$  m), however there is no higher entropy at  $Y = 5.205\text{e}6$  m, where fault 3 meets fault 2 (Fig. 10c)). Again, this is due to the lack of implementing terminating faults and will not be considered in further results. Some parts of the faults have a very low entropy, appr. at  $Y = 5.210\text{e}6$  m, not visible with this scale. The scope of higher entropy around the faults also changes. Fault 5 has a greater scope at the very top and around  $Y = 5.220\text{e}6$  m. Faults 3 and 4 have their greatest area of higher entropy (not considering mentioned area before) at  $Y = 5.200\text{e}6$  m.

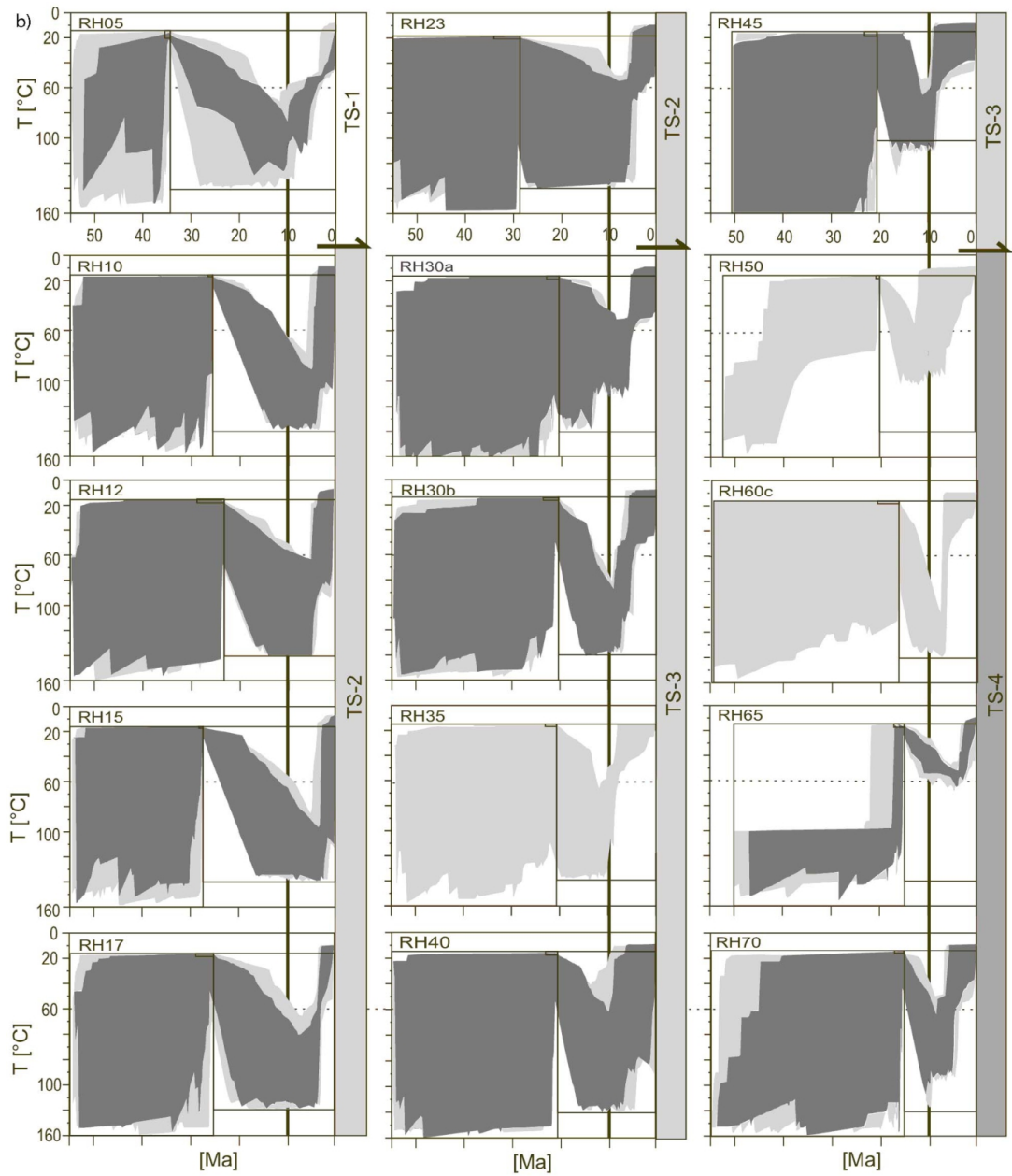


Figure 8: Thermal modeling results from HeFTy for the samples discussed. The dark grey path represents better fits ( $GOF > 0.5$ ), the light grey path less likely fits ( $GOF > 0.05$ ). The boxes mark the time of deposition and post- or prepositional temperature constraints. The thick line at 10 Ma marks a cooling event which occurred in nearly all samples. (From von Hagke et al. (2012))

Table 2: Maximum, mean and minimum entropy ( $H$ ) of the probabilistic model.

	max	mean	min
Lith. blocks	2.55	0.53	0.0
Fault blocks	3.00	0.08	0.0

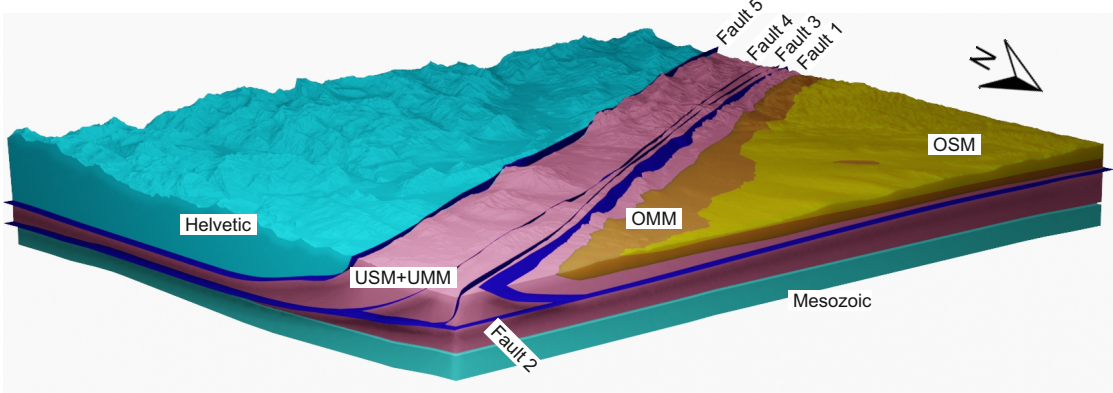


Figure 9: Geometric model of the subsurface of the study area computed with GemPy and processed with Blender.

Table 3: Exhumation at the base of each fault of kinematic models a) and b), see fig. 11 for realizations.

Model	Fault 1	Fault 2	Fault 3	Fault 4
a)	1.44 km	1.55 km	2.87 km	3.6 km
b)	1.44 km	1.55 km	3.20 km	3.5 km

### 3.2. Kinematic modeling

Overall, the kinematic models made with Noddy resemble the surface geology well, only the area north of the triangle zone is not in accordance with the geological map (Fig.11) (swisstopo). The outcropping thickness of OMM on fault 1 is too thin in all of the models, it should be approximately 1 km, but only ranges up to 700 m in the models. The same issues appeared with the adjacent USM. Both formation thicknesses depend on the geometry of fault 1, which thins the strata above, like in Fig. 6 b). Therefore no distinct exhumation value could be determined for fault 1 with this method. Assuming that fault 1 is merely bent upwards by the deformation of fault 2, an exhumation of at least 1.44 km must have occurred (see Tab. 3). The settings representing fault 2 are limited, only one was found which lead to the USM outcropping over the whole extent of the triangle zone. The exhumation value obtained is 1.55 km. The shape of the implemented fault however, does not represent a naturally occurring fault. It rather resembles a duplex structure, without indicating how many there really are. Implementing more duplex-like faults was not possible with Noddy due to its simplified set-up and lack of higher resolution to model the faults more precisely. For fault 3 the models imply a minimum exhumation of 2.87 km. When trying to obtain less exhumation by making the fault steeper, some OMM would remain underneath fault 4. Meaning fault 4 would also have to be steeper, resulting in a wrong surface geology. The minimum exhumation on fault 4 is 3.5 km. For further analysis a model was used combining the faults in table 3 with the least exhumation. All in all, the scope of variation in the shape of the faults is limited if the surface geology has to be kept the same.

The added lines of the faults in fig. 11 and 12 will not be precisely in this spot, since Noddy only shows the lithology and therefore only the effect of the faults. This limitation leads to incongruent reactivated faults or faults cutting through a different tectonic slice. These artifacts become visible when inserting the horizontal layer (see Fig. 12 b) c) f)).

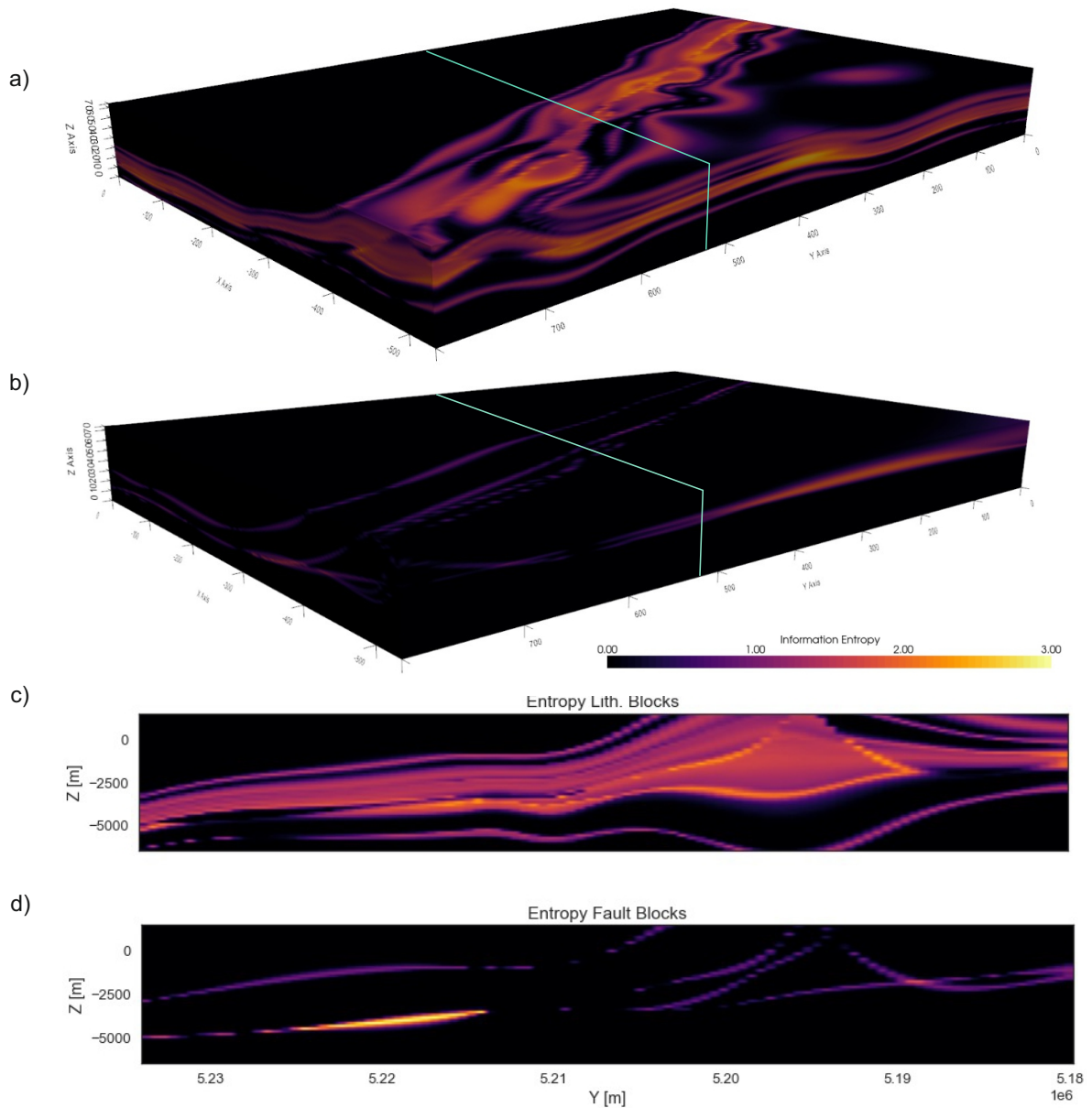


Figure 10: Visualization of the information entropy of the geometric model a) 3D lithology blocks of the whole extent b) 3D fault blocks model of the whole extent, c) profile section along the red line in a) showing the entropy of the lithology blocks, d) profile section along the red line in b) showing the entropy of the fault blocks.

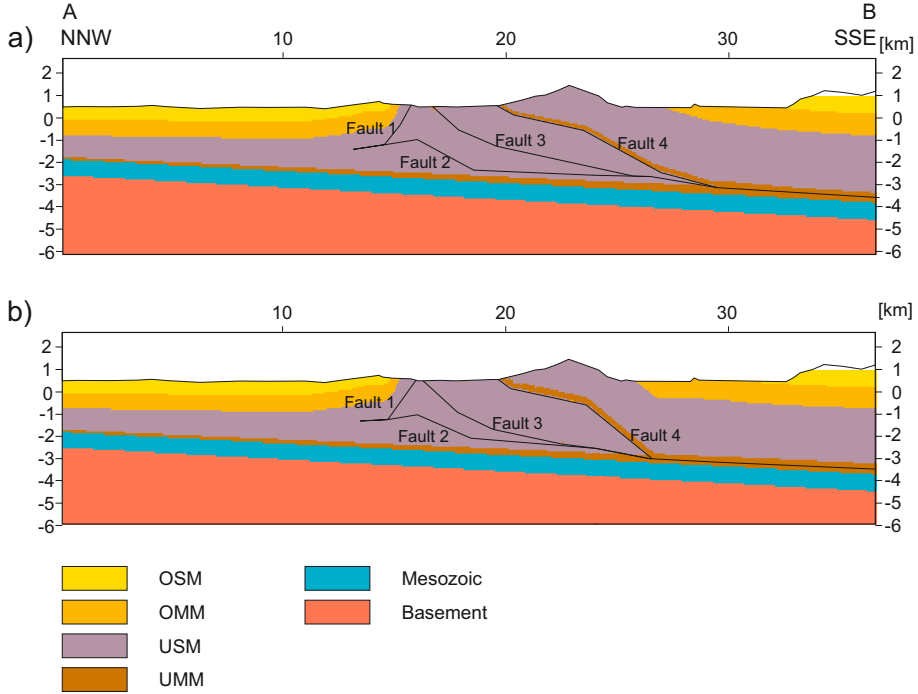


Figure 11: Two kinematic realizations made using Noddy with similar but different fault geometry and resulting exhumation. For the difference in exhumation see tab. 3.

### 3.3. Exhumation and cooling rates

The model in fig. 12 uses the fault settings which lead to the least exhumation. The horizontal layer inserted was used to trace at which depth the particle was before deformation took place. This depth was then used to calculate the resulting exhumation and the burial temperature according to the geothermal gradient (see Tab. 3.3). The exhumation values for RH50 and RH60c were obtained by measuring the distance to the top of the formation and then estimating the depth prior to deformation. The HeFTy models show the possible T-t paths of the samples (Fig. 8). They indicate a temperature to which the sample must have been heated at least, when it was buried the deepest. Assuming the cooling signal is only related to exhumation, this would be right before cooling started. These temperatures should be equal or lower than the estimated burial temperature. For  $GOF > 0.5$  this was not the case for samples RH10, RH12, RH15, RH30b, RH40, and RH45. Meaning the kinematic models do not indicate burial to such great depths as the thermochronological data suggests. In order to heat all samples to the temperature indicated in the HeFTy models a geothermal gradient of  $42^{\circ}\text{C}/\text{km}$  is necessary. The other samples (RH17, RH23, RH30a, RH35) lie within the suggested temperatures. For  $GOF > 0.05$ , samples RH10, RH12, RH30b, and RH45 are still outside the expected range of temperatures.

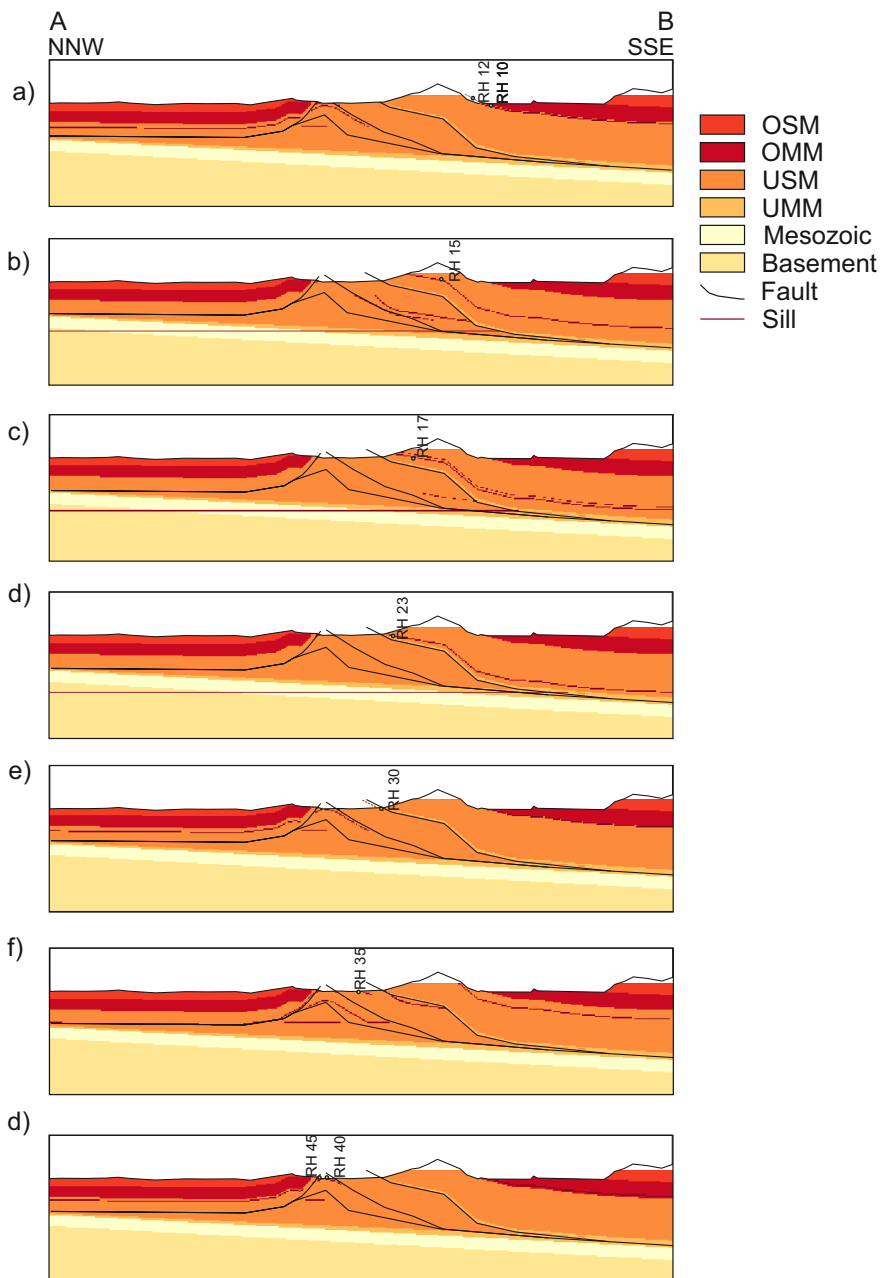


Figure 12: One kinematic realization with faults producing the least amount of exhumation, while staying true to the surface geology. Each figure uses a different depth of the horizontal layer to show the exhumation of the samples. For depth, elevation, and exhumation see Tab. 3.3

Table 4: Sample, elevation of sample, depth of horizontal layer before thrusting, exhumation, temperature at depth of horizontal layer, and minimum temperature the particle must have experienced before being exhumed (see Fig. 8). GOF: Goodness of fit.

Sample	TS	Elevation	Depth of	Exhumation	Temperature at depth	Min. temperature	
		(masl)	horizontal layer (masl)	(masl)	of horizontal layer (°C)	before exhumed (°C)	
RH60c	4	465	-700	1165	110	-	45
RH50	4	740	-1250	1990	55	-	70
RH45	3	535	-800	1335	50	65	55
RH40	3	550	-800	1350	50	65	40
RH35	3	562	-1550	2112	70	-	65
RH30a	3	475	-1025	1500	50	50	50
RH30b						85	80
RH23	2	383	-3150	3580	100	60	50
RH17	2	444	-2900	3344	95	80	65
RH15	2	630	-2675	3305	95	95	75
RH12	2	735	-925	1660	60	60	60
RH10	2	665	-925	1590	55	90	70

## 4. Discussion

### 4.1. Limitations in the modelling processes

#### 4.1.1. Geometric and probabilistic model

Although the GemPy model does not fully resemble the observed and expected geology, the faults are accurate enough for the probabilistic model, which gives valuable new information. The probabilistic model of the lithologies contains too many artifacts for further analysis, but in this case is also not of need for the next steps. Simplifying the geometric model further and choosing a smaller area would help concentrating on the more important structures and may help to minimize conflicting orientations. The model data set contains 333 orientations, most of them were computed using GemGIS, which also gave several wrong points and orientations. In the modeling process, several values were already excluded, but it is likely that there are still some interfering with each other. Starting with less orientations and adding more on the go would be a better approach than starting with many and deleting them. The interpolation by GemPy often does not give the expected results, to correct for this, additional data was used, which is considered expert knowledge. However, this introduces a great human factor as these points are biased.

The probabilistic model of the faults gives further insights on the likelihood of geometry and position of the faults. Looking at the whole extent, the highest entropy is in the north of the Entlebuch profile, where faults 1 and 2 are located. Since these faults terminate around 4 to 6 km north of the triangle zone, data points had to be invented in this area, which was kept to a minimum in order to reduce bias. Small deviations in these scarce position of these points can already produce a greater difference

than compared to areas with more input data. Another area of particularly high entropy is visible in the profile section where faults 2 and 4 part. Again, in the model there are more faults than in reality, because they could not be terminated. Having 3 faults in the same position means there are more possible outcomes per cell, which increases the entropy. Adding more data points would lower the entropy also in this case. These areas of high entropy will not be considered in the following discussion since they are not relevant or considered outliers. Since the entropy is a function of possible outcomes per cell, the minimized resolution in z has impacted the results. Using 100 cells instead of 50 would lower the entropy of the model. Furthermore, the assigned  $\sigma$  are considered expert knowledge and are a personal choice which can be argued with.

The scope of the faults entropy resembles their quantitative uncertainty, similar to an error bar. These areas were considered most relevant, next to areas of faults intersecting for the kinematic modeling process.

A limitation of this approach to estimate uncertainties is the lack of geologic realism in the random models. Making small changes in the GemPy input data set, especially in the structural more complex areas can produce artefacts which will show up in the entropy model. Furthermore, it only represents the uncertainties of one geologic realization chosen to model. Comparing the Rigi profile sections in fig. 4 b) and c) shows how greatly these can vary. Burkhard (1990) interpreted duplex units within the triangle zone, whereas Kaiser (2018) only incorporated a single ramp. Furthermore, faults 3 and 4 in the profile of fig. 4 b) have ramps integrated in contrast to more concave shaped faults in the other two publications. These very basic differences cannot be incorporated in the probabilistic modeling workflow. Overall, the quality of the resulting geometric and entropy model is limited to the quality of data used and, in this case, it gave rather a qualitative than quantitative estimation of uncertainties.

#### 4.1.2. Kinematic model

Considering the simplicity of Noddy, the surface geology could be represented well by the kinematic models, only the area north of the triangle zone could not be modeled and there exhumation was estimated using a different approach. The artifacts imply that tectonic slices have mixed, leading to exhumation of e.g. TS 3 in TS 4. This could be the case for fault 2 and fault 3, where the reactivated fault 3 is likely to not be at the exact position of the initial fault 3 and fault 2 may have cut through. The low resolution of Noddy's built-in line section function does not allow for exact calibration of the faults.

Modeling fault 2 with more than one fault (i.e. a duplex structure), as in Burkhard (1990), was not possible. But this could have a great impact on the exhumation rate. Trying a different software which makes it easier to implement duplex structures could give more insight into this. The exhumation value of 1.55 km on fault 2 is regarded as a minimum, since less exhumation meant that OMM was cropping out in the triangle zone. In this approach it was also the maximum because more exhumation left remnants of the OMM in the subsurface of the triangle zone. Therefore, exhumation is also limited by the pre-deformation thickness of the USM, which was assumed to be consistently growing towards the south of the basin. Samples RH40 and RH45 were, according to the Noddy model, buried to the same depth and also the HeFTY models suggest similar t-T paths. However, the

difference in the expected exhumation according to HeFTY and the modeled exhumation is about 500 m. The values for fault 3 and 4 are only a minimum, they could easily be greater. This depends on the slip applied to the fault, hence it is limited to the size of the basin prior to deformation.

Maybe the biggest limitation in the kinematic models is the human factor brought in by altering the faults by hand. This is in stark contrast to the approach of minimizing uncertainties in the implicit models. On the other side the alterations are more realistic in a geological sense, because they were done by a geologist and not by drawing random values. This way unrealistic models could be excluded.

However, including uncertainty in the exhumation rates would be an important next step. In this study it was only possible to find a minimum of shortening and exhumation. No distinct solution for a model with maximum exhumation could be found, because the slip on each fault can be arbitrarily great. Greater exhumation, while keeping a realistic surface geology, can be modeled by increasing the slip and increasing the distance between each faults. The maximum exhumation is therefore limited by the pre-deformation extent of the NAFB, making the scope of slip big.

## 4.2. Exhumation rates

The burial temperatures resulting from the obtained exhumation values are in 7 out of 12 samples lower than what their T-t path suggests (for GOF > 0.5) (Fig. 8, Tab. 3.3). The differences in the expected and measured temperatures are not minor, they reach up to 33.3°C (Sample RH10), meaning this particle is expected to have experienced 1.11 km more exhumation than the kinematic model suggests. For sample RH12 0.04 km more exhumation would be necessary, for RH15 0.01 km, for RH30b 1.04 km, and for RH40 0.52 km, for RH45 0.53 km, and for RH60c 2.2 km. Since the kinematic models with Noddy are not too precise, RH12 and RH15 are regarded to be within the scope of error.

Even when using GOF > 0.05, there are 4 samples where the cooling signal cannot be explained by tectonic shortening alone. Again RH12 is excluded because the difference of 40 m is regarded as within error.

The horizontal profile includes more samples, whose exhumation rate could not be modeled with Noddy (RH70, RH65, RH05) and where no t-T model was available (RH25, P025) (Fig. 13. In TS 4 the He ages are consistent, while the AFT ages vary a lot. Considering that sample RH70 did not experience any deformation, the age would be expected to be similar to sample RH65. According to von Hagke et al. (2012) RH70 was partially annealed, while RH65 and RH50 are not. RH60c is only made up of 6 single grain ages, however these grains are completely annealed. If RH60c was reset only due to burial and following exhumation, it must have been buried to depth of about 3.2 km. Such great exhumation is not supported by any of the models for this sample. Furthermore, the AFT and He ages of RH60c are inverted. According to the closing temperature the AFT age is expected to be older than the He age, if the He age is older than the AFT age they are considered inverted. Estimations on the amount of erosion that impacted the OSM cannot be made, therefore it is unclear how much of the cooling signal of samples RH65 and RH70 can be attributed to erosion.

In TS 3 the ages are more consistent than in TS 4. Samples RH40 and RH45 are both indicating 500 m more exhumation, here the geological model might be wrong. Samples RH35 and RH30a are

within the expected range of exhumation, only sample RH30b is not.

In TS 2, the most obvious outlier is P025 with an age of  $43.28 \pm 6.89$  Ma. Although no grain age distribution was available for this data point, the age does not imply any annealing. This is in stark contrast to the other samples in TS 2, which were all completely reset or annealed. Also here the Noddy model does not support cooling solely due to tectonic shortening for sample RH10. Although a thermal anomaly, due to the nearby fault overthrusting the Helvetic unit, could have impacted the recent cooling history, the difference in expected and modeled exhumation is great and therefore other factors must have played a role.

Sample P025 is also regarded as an outlier in the vertical profile (Fig. 14). This age is made up of 23 single grain ages making it a valuable data point. A t-T model is missing for this sample. The difference in the cooling ages of AFT samples in the same tectonic slice and similar elevation would suggest a fault in between, however there is no evidence supporting this. While the other ages in the vertical profile, besides data point S3c, fit to the expected exhumation of a paleo PAZ and PRZ this particle was not affected by reheating. S3c is one (U-Th-Sm)/He age of sample S3. The ages were not combined to one mean age and S3c was a broken crystal, hence there is higher uncertainty related to its age.

While a higher geothermal gradient could explain the thermochronological data at least to some extent, it does not seem feasible and there is no evidence supporting it. For samples with a great difference in observed and expected exhumation, such as RH10, the geothermal gradient would have to be as high as  $\nabla T = 47^\circ\text{C}/\text{km}$  (for GOF > 0.5). A higher geothermal gradient also does not explain the heterogeneous cooling signals in the same tectonic slices. In all modeled tectonic slices there are samples which fit into the expected exhumation rate and samples which don't. If a greater rate of tectonic shortening was responsible for the young ages, it would have to apply to all samples in one tectonic slice. Therefore, the heterogeneity of the cooling rates rather suggests a responsible process on smaller scale.

### 4.3. Processes influencing cooling rates

The mismatches in calculated and observed temperature indicate that the cooling signal is related to other processes than tectonic exhumation. Many assumptions on different drivers of cooling in the Subalpine Molasse have been made. Cederbom et al. (2004, 2011) argues that the remaining exhumation is a result of isostatic rebound due to wetter climate and hence more erosion. However, such large scale process cannot explain the thermal anomaly we see only at Rigi. Schlunegger and Mosar (2011) argue that the major part of erosion in the Molasse Basin was caused by a reorganization of drainage patterns controlled by tectonics in the Cenozoic European Rift System and climate change only occurred with the onset of the Quaternary ice ages. von Hagke et al. (2012) ascribes cooling up to  $-40^\circ\text{C}$ , equal to exhumation of 1–1.5 km, to glacial erosion. However, this is a maximum, strongly depending on the exact sample location. It is also important to keep in mind that the geothermal gradient and surface temperature used represent recent measurements. A suggested paleo geothermal gradient of as low as  $15^\circ\text{C}$  would be plausible for the area around Rigi, meaning that even more cooling may not be explained by exhumation linked to tectonic processes (Cederbom et al., 2011).

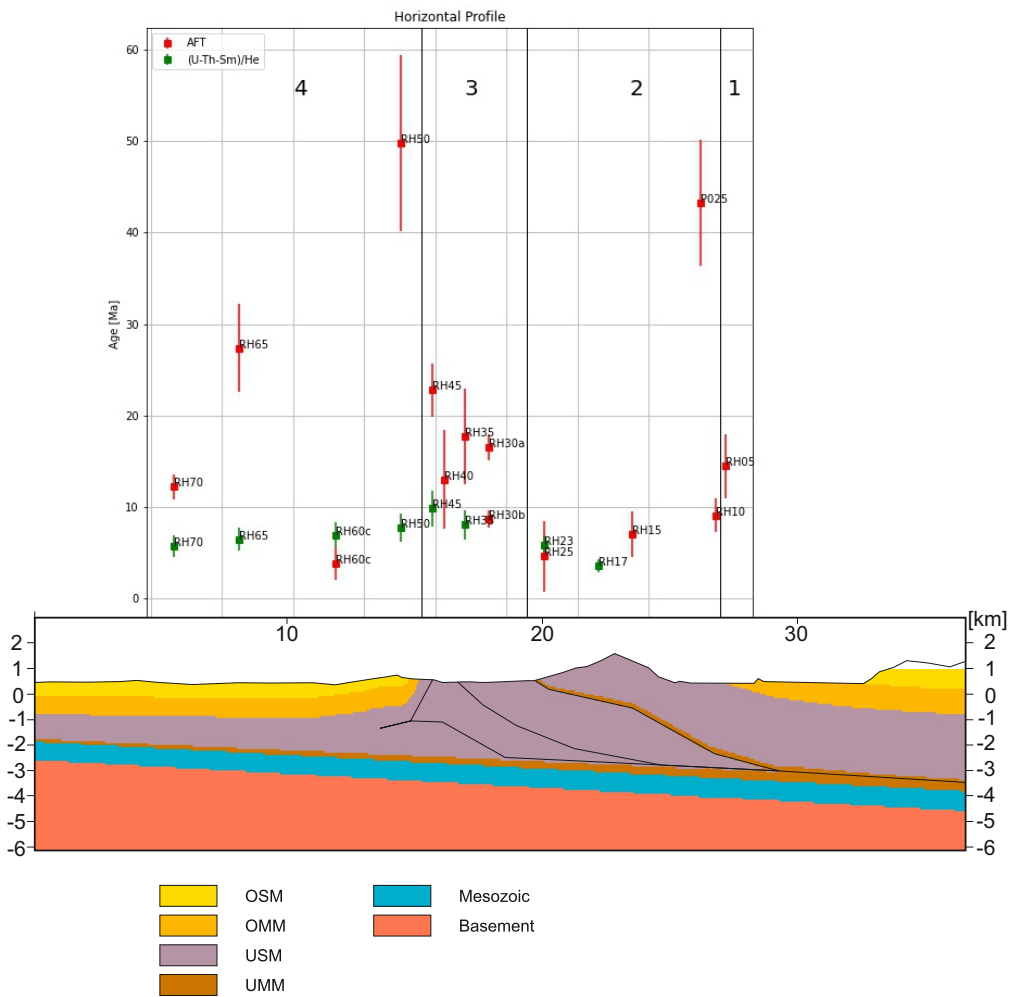


Figure 13: AFT and (U-Th-Sm)/He data plotted along the profile section. The numbers 1–4 refer to the tectonic slice. Data from Cederbom et al. (2004); von Hagke et al. (2012); Lindow (2009)

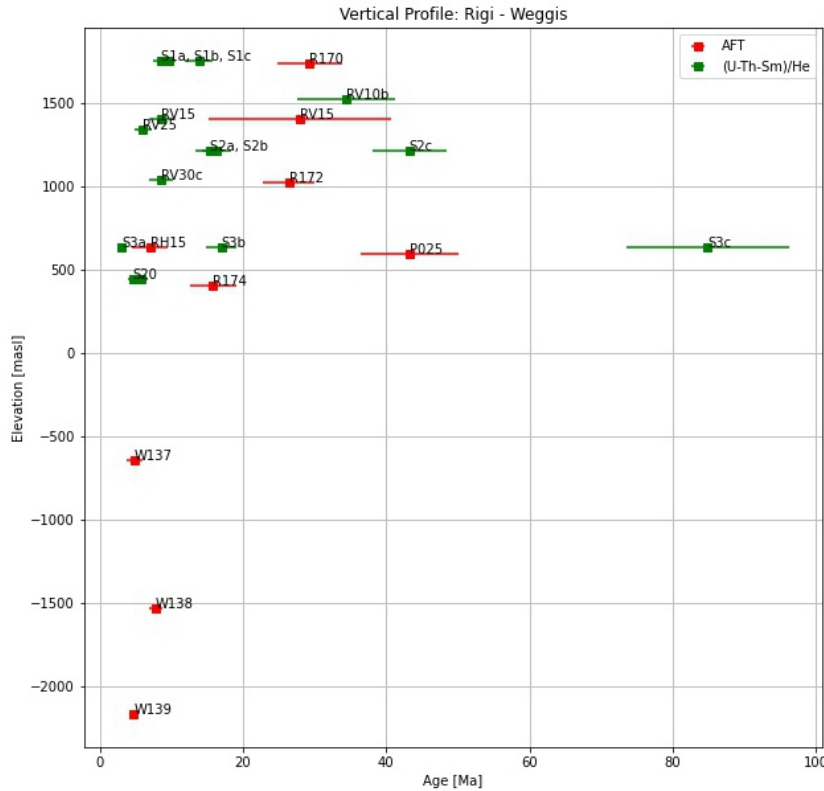


Figure 14: AFT and (U-Th-Sm)/He data plotted against elevation. Data from Cederbom et al. (2004); von Hagke et al. (2012); Lindow (2009)

Glacial erosion has also been discussed as a potential reason for the difference in cooling rates (von Hagke et al., 2012). While this could explain different cooling rates in different locations, it does not explain differences in burial depth only a change in the cooling signal with the onset of the Quaternary ice ages. Another process related to cooling is hydrothermal flow. This could account for cooling on smaller scale and is not unusual in tectonic active regimes.

#### 4.4. Hydrothermal flow in triangle zones and foreland basins

Sedimentary basins, such as the Molasse basin, are a common target of deep geothermal exploration (Chelle-Michou et al., 2017; Rybach, 1992). In the NAFB the mesozoic underlying carbonates are the primary target formation (Heuberger et al., 2016). Hydrothermal fluids can travel upwards along faults, if the aquifer cut by the fault is confined (Taillefer et al., 2017). The UMM is due to its lithology an impermeable stratum, while the underlying Jurassic carbonate is often carstified and therefore an excellent aquifer (Rybach, 1992; Chelle-Michou et al., 2017). In all geological profiles in fig. 4 faults cutting through the Mesozoic layers and the UMM are indicated. This implies that fluids from greater depths have a possibility to reach shallower units. Depending on the temperatures and flow rates, the geothermal gradient could be greater than assumed in these areas giving a possible explanation to the thermochronological ages not explained by tectonic shortening.

#### **4.5. Alteration of thermochronometers through hydrothermal fluids**

Depending on the flow rate, duration, and temperature, hydrothermal flow can affect the ages measured of thermochronometers (Berger et al., 2022; Luijendijk, 2019; Milesi et al., 2020; Whipp Jr and Ehlers, 2007). If not taken into account, this will falsify further interpretations or in this case exhumation rates. The (U-Th-Sm)/He system of apatites close to faults can be divided into three different groups: a) apatites matching the regional cooling trend, unaffected by hydrothermal flow, b) crystals younger than the regional cooling trend, and c) crystals with macroscopically non-visible fractures leading to trapping gain or diffusive loss of He, resulting in older or younger ages (Berger et al., 2022). Apatites from group b with a young age can either have been influenced by diffusive He loss due to reheating or they can have recrystallized from circulating hydrothermal fluids. Recrystallized apatites can be distinguished by having a different REE composition or lower Sm and Y concentrations (Berger et al., 2022). Apatites older than the regional trend (Group c) may also be influenced by upwelling He-bearing fluids and apatite precipitation leading to a higher He concentration (Berger et al., 2022). This is one possible scenario leading to inverted older He ages than AFT in a sample. There are also indications that inverted ages are related to rapid cooling (Spiegel et al., 2009). Rapid cooling is suggested by the HeFTy model for sample RH60c, which also features inverted ages.

### **5. Conclusion and outlook**

Taking structural uncertainties into account when working with thermochronological data has shown to provide new ways of interpretation. In this case it gave new implications on heatflow in the Swiss Subalpine Molasse and also implies that thermochronological data in settings with potential hydrothermal flow could more often have been misinterpreted. While structural uncertainties could be reduced to some extent, there still are areas of great uncertainty. Going back to the geometric model and using the new kinematic profile as input data could help reduce these uncertainties, as it contains more information on geological concepts. Applying the same steps to the other profile section used for the geometric model could then minimize the entropy of the whole model. Another important step would be to stochastically alter the Noddy model while automatically excluding models not true to surface geology. Furthermore, a numeric or analogue model of the area would provide valuable information to diminish structural uncertainties (Couzens-Schultz et al., 2003; Koyi and Sans, 2006). In order to get a better understanding of how hydrothermal flow may have affected thermochronological ages in the Swiss Subalpine Molasse the samples should be further evaluated, especially considering their REE, Sm, and Y concentrations.

The main findings of this work are:

- Although limited, GemPy is a powerful tool to estimate uncertainties in structural models
- Structural uncertainty in the geometric model is greatest in structural complex areas, such as faults cutting through layers or where faults intersect
- In this case, the approach of assessing uncertainties with GemPy gave rather qualitative than quantitative results

- Noddy is not fit for modeling such structural complex geological settings in high resolution
- The geometry of faults have an impact on the resulting exhumation, testing different geological frameworks could be a next step to constrain exhumation further
- Accounting for structural uncertainties in thermokinematic models helps to constrain the cooling signal related to tectonic shortening
- The cooling rate of at least 4 samples in von Hagke et al. (2012) (RH10, RH30b, RH45, RH60c) cannot be explained solely by tectonic shortening
- The heterogeneous distribution of plausible and implausible thermochronological data throughout the different tectonic slices suggests a driver of cooling on smaller scale, for example hydrothermal flow

*Supplementary material:* All supplementary material can be found in my GitHub repository:  
<https://github.com/JosefineZiegler/Master-Thesis>

## References

- Ph A Allen, M Mange-Rajetzky, Albert Matter, and P Homewood. Dynamic palaeogeography of the open Burdigalian seaway, Swiss Molasse basin. *Eclogae Geologicae Helvetiae*, 78(2):351–381, 1985.
- Philip A Allen and Peter Homewood. *Foreland basins*. John Wiley & Sons, 2009.
- Robin P Allenbach. *GeoMol: Geologisches 3D-Modell des Schweizer Molassebeckens: Schlussbericht*. Bundesamt für Landestopographie swisstopo, 2017.
- George Bárdossy and János Fodor. Traditional and new ways to handle uncertainty in geology. *Natural Resources Research*, 10(3):179–187, 2001.
- Alfons Berger and Romain Bousquet. Subduction-related metamorphism in the Alps: review of isotopic ages based on petrology and their geodynamic consequences. *Geological Society, London, Special Publications*, 298(1):117–144, 2008.
- Alfons Berger, Daniel Egli, Christoph Glotzbach, Pierre G Valla, Thomas Pettke, and Marco Herwegh. Apatite low-temperature chronometry and microstructures across a hydrothermally active fault zone. *Chemical geology*, 588:120633, 2022.
- Clare E Bond. Uncertainty in structural interpretation: Lessons to be learnt. *Journal of Structural Geology*, 74:185–200, 2015.
- Christian Brandes and David C Tanner. Fault-related folding: A review of kinematic models and their application. *Earth-Science Reviews*, 138:352–370, 2014.
- Sofia Brisson, Florian Wellmann, Nils Chudalla, Jan von Harten, and Christoph von Hagke. Estimating Uncertainties in 3-D Models of Complex Fold-and-Thrust Belts: A Case Study of the Eastern Alps Triangle Zone. Available at SSRN 4274454, N.D. unpublished.
- Martin Burkhard. Aspects of the large-scale Miocene deformation in the most external part of the Swiss Alps (sub-Alpine molasse to Jura fold belt). *Eclogae Geologicae Helvetiae*, 83(3):559–583, 1990.
- William D Carlson, Raymond A Donelick, and Richard A Ketcham. Variability of apatite fission-track annealing kinetics: I. Experimental results. *American mineralogist*, 84(9):1213–1223, 1999.
- Charlotte E Cederbom, Hugh D Sinclair, Fritz Schlunegger, and Meinert K Rahn. Climate-induced rebound and exhumation of the European Alps. *Geology*, 32(8):709–712, 2004.
- Charlotte E Cederbom, Peter van der Beek, Fritz Schlunegger, Hugh D Sinclair, and Onno Oncken. Rapid extensive erosion of the North Alpine foreland basin at 5–4 Ma. *Basin Research*, 23(5): 528–550, 2011.
- Cyril Chelle-Michou, Damien Do Couto, Andrea Moscariello, Philippe Renard, and Elme Rusillon. Geothermal state of the deep western Alpine Molasse basin, France-Switzerland. *Geothermics*, 67: 48–65, 2017.

David M Chew and Richard A Spikings. Geochronology and thermochronology using apatite: time and temperature, lower crust to surface. *Elements*, 11(3):189–194, 2015.

Brent A Couzens-Schultz, Bruno C Vendeville, and David V Wiltschko. Duplex style and triangle zone formation: insights from physical modeling. *Journal of Structural Geology*, 25(10):1623–1644, 2003.

Miguel de la Varga, Alexander Schaaf, and Florian Wellmann. GemPy 1.0: open-source stochastic geological modeling and inversion. *Geoscientific Model Development*, 12(1):1–32, 2019.

Zoltán Erdős, Peter van der Beek, and Ritske S Huismans. Evaluating balanced section restoration with thermochronology data: A case study from the Central Pyrenees. *Tectonics*, 33(5):617–634, 2014.

PG Fitzgerald, Suzanne L Baldwin, LE Webb, and Paul B O’Sullivan. Interpretation of (U-Th)/He single grain ages from slowly cooled crustal terranes: a case study from the Transantarctic Mountains of southern Victoria Land. *Chemical Geology*, 225(1-2):91–120, 2006.

W Frisch. Tectonic progradation and plate tectonic evolution of the Alps. *Tectonophysics*, 60(3-4):121–139, 1979.

G Gehrels, P Kapp, P DeCelles, A Pullen, R Blakey, A Weislogel, Lin Ding, J Guynn, A Martin, N McQuarrie, et al. Detrital zircon geochronology of pre-Tertiary strata in the Tibetan-Himalayan orogen. *Tectonics*, 30(5), 2011.

E Greber, T Grünenfelder, B Keller, and R Wyss. Die Geothermie-Bohrung Weggis, Kanton Luzern. *Bulletin der Vereinigung Schweizerischer Petroleum-Geologen und-Ingenieure*, 61(138):17–43, 1994.

Stefan Heuberger, Philippe Roth, Olivier Zingg, Henry Naef, and Beat P Meier. The St. Gallen Fault Zone: a long-lived, multiphase structure in the North Alpine Foreland Basin revealed by 3D seismic data. *Swiss Journal of Geosciences*, 109(1):83–102, 2016.

Arnold Rudolf Holliger. Geologische Untersuchungen der subalpinen Molasse und des Alpenrandes in der Gegend von Flühli, Entlebuch, Kt. Luzern. Verkürzte Fassung der Inauguraldissertation, etc.[With maps.]. *Eclogae Geologicae Helvetiae*, 48(1):79–98, 1955.

Peter Homewood, PA Allen, and GD Williams. Dynamics of the Molasse Basin of western Switzerland. In *Foreland basins*, volume 8, pages 199–217. Blackwell Scientific Publications Oxford, UK, 1986.

Mark Jessel. “Noddy” – An interactive Map creation Package. Master’s thesis, Imperial College of Science and Technology, London, UK,, 1981.

Mark Jessell, Laurent Aillères, Eric De Kemp, Mark Lindsay, Florian Wellmann, Michael Hillier, Gautier Laurent, Thomas Carmichael, and Roland Martin. Next generation three-dimensional geologic modeling and inversion. *Society of Economic Geologists*, 18:261–272, 2014.

- Mark W Jessell and Rick K Valenta. Structural geophysics: Integrated structural and geophysical modelling. In *Computer methods in the geosciences*, volume 15, pages 303–324. Elsevier, 1996.
- Alexander Juestel, Arthur Correira Endlein, Florian Wellmann, and Marius Pischke. GemGIS – GemPy Geographic: Open-Source Spatial Data Processing for Geological Modeling, 2021. URL <https://doi.org/10.5194/egusphere-egu21-4613>. EGU General Assembly 2021.
- Leonard Kaiser. Restoring the Central Alps including uncertainty analysis: an orogeny scale cross section from the eastern Jura into the External Crystalline Massifs. Master’s thesis, RWTH Aachen, 2018.
- Richard A Ketcham. Forward and inverse modeling of low-temperature thermochronometry data. *Reviews in mineralogy and geochemistry*, 58(1):275–314, 2005.
- Hemin A Koyi and Maura Sans. Deformation transfer in viscous detachments: comparison of sandbox models to the South Pyrenean Triangle Zone. *Geological Society, London, Special Publications*, 253(1):117–134, 2006.
- Christian Lajaunie, Gabriel Courrioux, and Laurent Manuel. Foliation fields and 3D cartography in geology: principles of a method based on potential interpolation. *Mathematical Geology*, 29(4): 571–584, 1997.
- Julia Lindow. *Insights on Plio-Pleistocene tectonics within the Swiss Subalpine Molasse using low-temperature thermochronology and structural analyses along the Rigi transect (Central Switzerland)*. PhD thesis, University of Potsdam, 2009.
- Elco Luijendijk. Beo v1. 0: numerical model of heat flow and low-temperature thermochronology in hydrothermal systems. *Geoscientific Model Development*, 12(9):4061–4073, 2019.
- KR McClay. Glossary of thrust tectonics terms. *Thrust tectonics*, pages 419–433, 1992.
- Nadine McQuarrie, Delores Robinson, Sean Long, Tobgay Tobgay, Djordje Grujic, George Gehrels, and Mihai Ducea. Preliminary stratigraphic and structural architecture of Bhutan: Implications for the along strike architecture of the Himalayan system. *Earth and Planetary Science Letters*, 272 (1-2):105–117, 2008.
- MeteoSwiss. Klimanormwerte Temperatur 1991-2020. URL <https://www.geocat.ch/geonetwork/srv/ger/catalog.search#/metadata/68adbf85-b4b1-4ce6-9c1c-e7b895d885ec>.
- Gaétan Milesi, Patrick Monié, Philippe Münch, Roger Soliva, Audrey Taillefer, Olivier Bruguier, Mathieu Bellanger, Michaël Bonno, and Céline Martin. Tracking geothermal anomalies along a crustal fault using (U- Th)/ He apatite thermochronology and rare-earth element (REE) analyses: the example of the Têt fault (Pyrenees, France). *Solid Earth*, 11(5):1747–1771, 2020.
- Andrew J Newell. Implicit geological modelling: a new approach to 3D volumetric national-scale geological models. 2018.
- N Okaya, R Freeman, E Kissling, and St Mueller. A lithospheric cross-section through the Swiss Alps—I. Thermokinematic modelling of the Neoalpine orogeny. *Geophysical Journal International*, 125(2):504–518, 1996.

- O Adrian Pfiffner. *Geologie der Alpen*, volume 8416. UTB, 2015.
- Peter W Reiners and Todd A Ehlers. *Low-Temperature Thermochronology:: Techniques, Interpretations, and Applications*, volume 58. Walter de Gruyter GmbH & Co KG, 2018.
- Gideon Rosenbaum, Gordon S Lister, and Cécile Duboz. Relative motions of Africa, Iberia and Europe during Alpine orogeny. *Tectonophysics*, 359(1-2):117–129, 2002.
- Ladislaus Rybach. Geothermal potential of the Swiss Molasse basin. *Eclogae Geologicae Helvetiae*, 85(3):733–744, 1992.
- Alexander Schaaf and Clare E Bond. Quantification of uncertainty in 3-D seismic interpretation: implications for deterministic and stochastic geomodeling and machine learning. *Solid earth*, 10(4):1049–1061, 2019.
- Fritz Schlunegger. Controls of surface erosion on the evolution of the Alps: constraints from the stratigraphies of the adjacent foreland basins. *International Journal of Earth Sciences*, 88(2):285–304, 1999.
- Fritz Schlunegger and Jon Mosar. The last erosional stage of the Molasse Basin and the Alps. *International Journal of Earth Sciences*, 100:1147–1162, 2011.
- Fritz Schlunegger, Albert Matter, DW Burbank, and EM Klaper. Magnetostratigraphic constraints on relationships between evolution of the central Swiss Molasse basin and Alpine orogenic events. *Geological Society of America Bulletin*, 109(2):225–241, 1997.
- Herbert Scholz. *Bau und Werden der Allgäuer Landschaft*. Schweizerbart’sche Verlagsbuchhandlung, 2016.
- SEAG. Hünenberg 1. URL [https://api3.geo.admin.ch/rest/services/geol/MapServer/ch.swisstopo.geologie-bohrungen\\_tiefer\\_500/813/extendedHtmlPopup?lang=de](https://api3.geo.admin.ch/rest/services/geol/MapServer/ch.swisstopo.geologie-bohrungen_tiefer_500/813/extendedHtmlPopup?lang=de).
- Claude Elwood Shannon. A mathematical theory of communication. *ACM SIGMOBILE mobile computing and communications review*, 5(1):3–55, 2001.
- Martine Simoes, Jean Philippe Avouac, Olivier Beyssac, Bruno Goffé, Kenneth A Farley, and Yue-Gau Chen. Mountain building in Taiwan: A thermokinematic model. *Journal of Geophysical Research: Solid Earth*, 112(B11), 2007.
- HD Sinclair. Tectonostratigraphic model for underfilled peripheral foreland basins: An Alpine perspective. *Geological Society of America Bulletin*, 109(3):324–346, 1997.
- HD Sinclair, BJ Coakley, PA Allen, and AB Watts. Simulation of foreland basin stratigraphy using a diffusion model of mountain belt uplift and erosion: an example from the central Alps, Switzerland. *Tectonics*, 10(3):599–620, 1991.
- Cornelia Spiegel, Barry Kohn, David Belton, Zsolt Berner, and Andrew Gleadow. Apatite (U–Th–Sm)/He thermochronology of rapidly cooled samples: the effect of He implantation. *Earth and Planetary Science Letters*, 285(1-2):105–114, 2009.

Bundesamt für Landestopografie swisstopo. Geologische Vektordatensätze GeoCover.  
URL <https://map.geo.admin.ch/mobile.html?topic=geol&lang=de&bgLayer=ch.swisstopo.pixelkarte-grau&layers=ch.swisstopo.geologie-geocover>.

Audrey Taillefer, Roger Soliva, Laurent Guillou-Frottier, Elisabeth Le Goff, Guillaume Martin, and Michel Seranne. Fault-related controls on upward hydrothermal flow: an integrated geological study of the Têt fault system, Eastern Pyrénées (France). *Geofluids*, 2017, 2017.

Pierre Tricart. From passive margin to continental collision; a tectonic scenario for the Western Alps. *American Journal of Science*, 284(2):97–120, 1984.

Rudolf Trümpy. Paleotectonic evolution of the Central and Western Alps. *Geological Society of America Bulletin*, 71(6):843–907, 1960.

Rudolf Trümpy et al. *Geology of Switzerland. A: An outline of the geology of Switzerland*. Wepf & Co, 1980.

Pieter Vermeesch and Yuntao Tian. Thermal history modelling: HeFTy vs. QTQt. *Earth-Science Reviews*, 139:279–290, 2014.

C von Hagke, CE Cederbom, Onno Oncken, DF Stöckli, MK Rahn, and F Schlunegger. Linking the northern Alps with their foreland: The latest exhumation history resolved by low-temperature thermochronology. *Tectonics*, 31(5), 2012.

Christoph von Hagke and Alexander Malz. Triangle zones–Geometry, kinematics, mechanics, and the need for appreciation of uncertainties. *Earth-Science Reviews*, 177:24–42, 2018.

Christoph von Hagke, E Luijendijk, Robert Ondrák, and Julia Lindow. Quantifying erosion rates in the Molasse basin using a high resolution data set and a new thermal model. In *20th International Conference on Deformation Mechanisms, Rheology & Tectonics*, pages 94–97. Schweizerbart Science Publishers, 2015.

Florian Wellmann and Guillaume Caumon. 3-D Structural geological models: Concepts, methods, and uncertainties. In *Advances in Geophysics*, volume 59, pages 1–121. Elsevier, 2018.

Florian Wellmann and Klaus Regenauer-Lieb. Uncertainties have a meaning: Information entropy as a quality measure for 3-D geological models. *Tectonophysics*, 526:207–216, 2012.

Florian Wellmann, Franklin G Horowitz, Eva Schill, and Klaus Regenauer-Lieb. Towards incorporating uncertainty of structural data in 3D geological inversion. *Tectonophysics*, 490(3-4):141–151, 2010.

Florian Wellmann, Sam T Thiele, Mark D Lindsay, and Mark W Jessell. pynoddy 1.0: an experimental platform for automated 3-D kinematic and potential field modelling. *Geoscientific Model Development*, 9(3):1019–1035, 2016.

David M Whipp Jr and Todd A Ehlers. Influence of groundwater flow on thermochronometer-derived exhumation rates in the central Nepalese Himalaya. *Geology*, 35(9):851–854, 2007.

## A. Raw GemPy model

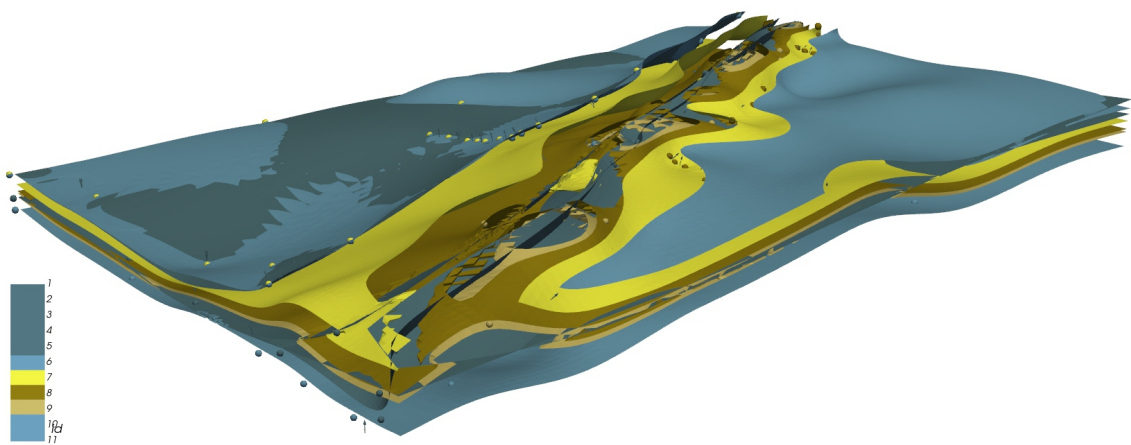


Figure 15: GemPy model before being processed with Blender

## B. Thermochronological Data

Table 5: Thermochronological data used in this study

Reference	Sample	Elevation (masl)	Type	Age (Ma)	Error (Ma)
von Hagke et al. (2012)	RH05	620	AFT	14.5	3.5
	RH05	620	He	3.57	0.71
	RH10	665	AFT	9.1	1.8
	RH12	735	He	4.29	0.86
	RH15	630	AFT	7	2.5
	RH17	461	He	3.59	0.72
	RH23	383	He	5.8	1.16
	RH25	430	AFT	4.6	3.9
	RH30a	475	AFT	16.5	1.4
	RH30b	475	AFT	8.7	1
	RH35	562	AFT	17.7	5.2
	RH35	562	He	8.08	1.62
	RH40	550	AFT	13	5.4
	RH45	535	AFT	22.8	2.9
	RH45	535	He	9.86	1.97
	RH50	740	AFT	49.8	9.6
	RH50	740	He	7.69	1.54
	RH60c	465	AFT	3.8	1.8
	RH60c	465	He	6.97	1.39
	RH65	450	AFT	27.4	4.8
	RH65	450	He	6.49	1.3
	RH70	523	AFT	12.2	1.4
	RH70	523	He	5.73	1.15
	RV10b	1520	He	34.35	6.87
	RV15	1405	AFT	8.54	1.71
	P025	590	AFT	43.28	6.89
Cederbom et al. (2004)	R170	1731	AFT	29.3	4.5
	R172	1024	AFT	26.4	3.6
	R174	402	AFT	15.8	3.3
	W137	-643	AFT	4.8	1.1
	W138	-1533	AFT	7.8	0.9
	W139	-2169	AFT	4.7	0.6